Available online at www.sciencedirect.com

ScienceDirect

Nuclear Physics B 960 (2020) 115203

NUCLEAR PHYSICS B

www.elsevier.com/locate/nuclphysb

Purely triplet seesaw and leptogenesis within cosmological bound, dark matter, and vacuum stability

Mina Ketan Parida [a,*], Mainak Chakraborty [b], Swaraj Kumar Nanda [a], Riyanka Samantaray [a]

[a] *Centre of Excellence in Theoretical and Mathematical Sciences, Siksha 'O' Anusandhan, Deemed to be University, Khandagiri Square, Bhubaneswar 751030, India*

[b] *Department of Physics, University of Calcutta, 92 Acharya Prafulla Chandra Road, Kolkata 700009, India*

Received 4 June 2020; received in revised form 24 September 2020; accepted 25 September 2020
Available online 29 September 2020
Editor: Tommy Ohlsson

Abstract

In a novel standard model extension it has been suggested that, even in the absence of right-handed neutrinos and type-I seesaw, purely triplet leptogenesis leading to baryon asymmetry of the universe can be realized by two heavy Higgs triplets which also provide type-II seesaw ansatz for neutrino masses. In this work we discuss this model predictions for hierarchical neutrino masses in concordance with recently determined cosmological bounds and oscillation data including θ_{23} in the second octant and large Dirac CP phases. We find that for both normal and inverted orderings, the model fits the oscillation data with the sum of the three neutrino masses consistent with current cosmological bounds determined from Planck satellite data. In addition, using this model ansatz for CP-asymmetry and solutions of Boltzmann equations, we also show how successful predictions of baryon asymmetry emerges in the cases of both unflavoured and two-flavoured leptogeneses. With additional Z_2 discrete symmetry, a minimal extension of this model is further shown to predict a scalar singlet WIMP dark matter in agreement with direct and indirect observations which also resolves the issue of vacuum instability persisting in the original model. Although the combined constraints due to relic density and direct detection cross section allow this scalar singlet dark matter mass to be $m_\xi = 750$ GeV, the additional vacuum stability constraint pushes this limiting value to $m_\xi = 1.3$ TeV which is verifiable by ongoing experiments. We also discuss constraint on the model parameters for the radiative stability of the standard Higgs mass.

* Corresponding author.
E-mail addresses: minaparida@soa.ac.in (M.K. Parida), mainak.chakraborty2@gmail.com (M. Chakraborty), swarajnanda.phy@gmail.com (S.K. Nanda), riyankasamantaray59@gmail.com (R. Samantaray).

https://doi.org/10.1016/j.nuclphysb.2020.115203

1. Introduction

Neutrino oscillation [1–3], baryon asymmetry of the universe [4,5] and dark matter [6] are the three most prominent physics issues which can not be explained within the purview of the standard model (SM). However, seesaw mechanisms have been widely recognized as possible origins of tiny neutrino masses where leptogenesis caused by the decay of mediating heavy particles are believed to be the underlying sources of baryon asymmetry through sphaleron interactions [7]. Large number of leptogenesis models using right-handed neutrino (RHN) mediated type-I seesaw [8–10], or other seesaw mechanisms, have been proposed for successful baryon asymmetry generation and a partial list of such extensive investigations is given in [11–14]. Since SM itself does not have RHNs, it has to be extended for the implementation of type-I seesaw. But, in a novel interesting proposal against the conventional lore and without using any RHNs or supersymmetry, realisation of neutrino masses and baryon asymmetry have been also shown to be possible [15] through the SM extension by two heavy scalar triplets, Δ_1 and Δ_2, each of which generates neutrino mass by another popular mechanism, called type-II seesaw [16]. The tree level dilepton decay of any one of these triplets combined with loop contribution generated by their collaboration predicts the desired CP-asymmetry formula for leptogenesis leading to observed baryon asymmetry of the Universe (BAU). In an implementation of this leptogenesis idea [15] in non-supersymmetric (non-SUSY) SM extension in the scalar sector, quasi-degenerate (QD) neutrino masses of order ~ 1 eV and solution to simplified Boltzmann equations have been used to predict the baryon asymmetry of the Universe $Y_B \sim 10^{-11}$. Leptogenesis with or without RHNs has been also implemented including or excluding supersymmetry [12,17–24]. The QD neutrino mass hypothesis used in [15] has also a very interesting outcome of predicting neutrinoless double beta decay rates [25], radiative magnification of neutrino mixings [26], and unification of quark and neutrino mixings at high scales [27]. On the other hand recent Planck satellite data [5] have set the cosmological upper bound on the sum of three light neutrino masses

$$\sum m_i \leq 0.23 \text{ eV} \equiv \Sigma_{Planck}, \tag{1}$$

which is consistent with the standard ΛCDM big bang cosmology of the Universe [5]. Although Planck satellite data [5] also permits a much larger value $\Sigma_C \simeq 0.71$ eV, this latter type of solution has been shown to be possible only in the absence of the cosmological constant (Λ). Compared to Planck satellite data [5], somewhat lower value of the cosmological bound $\Sigma_{new} = 0.12$ eV in the ΛCDM model has been also noted [28]

$$\sum m_i \leq 0.12 \text{ eV} \equiv \Sigma_{new}. \tag{2}$$

Sensitivity of non-standard interactions to neutrino masses has been investigated [29]. As against such cosmological bounds of eq. (1) and eq. (2), KATRIN Collaboration [30] has recently set the upper limit on the neutrino mass scale $m_0 \leq 1$ eV which predicts for QD neutrinos

$$\sum m_i \leq 3 \text{ eV} \equiv \Sigma_{\text{KATRIN}}. \tag{3}$$

For a QD neutrino mass scale as low as $m_0 \simeq 0.2$ eV or heavier, the neutrino would manifest in the direct experimental detection of neutrinoless double beta decay [25] establishing its Majorana

nature which has remained elusive so far. In any case it is quite important to investigate the impact of the cosmological bounds [5,28] and the recently measured neutrino oscillation data [1–3] on the two-Higgs triplet seesaw and purely triplet leptogenesis [15] in the absence of RHNs.

Quite recently certain new features have been revealed in the neutrino oscillation data [1–3] which have to be explained in any theoretical model. The new data reveal the values on atmospheric neutrino mixing angle to be in the second octant with $\theta_{23} \simeq 49.6^\circ$ and the Dirac CP phase to be large, $\delta \sim 214^\circ$. The impact of new cosmological bounds [5,28] or the new oscillation data [1–3] have not been examined on the triplet leptogenesis model [15,31,32]. On the other hand, type-II seesaw dominance in SO(10) with scalar dark matter and vacuum stability has been shown to be capable of providing excellent representation of the neutrino data [33] where RHN loop mediated triplet leptogenesis explains the baryon asymmetry of the universe. Unlike type-I seesaw, the type-II seesaw dominant mass matrix elements have one-to-one correspondence with the mass matrix constructed using the oscillation data, a fact which underlines the importance of type-II over type-I. The model under discussion [15] has the property of predicting two different type-II seesaw mass matrices mediated by the respective heavy triplets and has the ability that one of them can dominate over the other. In fact this type-II seesaw dominance property has been utilized in the original model [15] with quasi-degenerate neutrino masses. It is, therefore, quite pertinent to examine whether the seesaw model [15] can fit the current neutrino data [1–3] for hierarchical neutrino masses satisfying the cosmological bounds [5,28] while successfully predicting the observed baryon asymmetry of the universe.

Supersymmetric type-I seesaw leptogenesis with RHN mass scale $M_N \geq 10^9$ GeV [34] is known to predict over-production of gravitinos in the early universe affecting relic abundance of light elements. Resolution of gravitino problem [35] in the supersymmetric triplet seesaw model has been discussed [17]. A clear advantage of non-supersymmetric (non-SUSY) leptogenesis models including [15] is the absence of the gravitino problem ensuring cosmologically safe relic abundance [35]. On the other hand, the SM Higgs mass (m_ϕ) in [15] is not protected against radiative correction which is likely to give $\delta m_\phi \simeq 10^{13}$ GeV = the heaviest triplet mass in the model [36] tending to destabilise the electroweak gauge hierarchy. This calls for exploring fine-tuned naturalness (or stability) constraint on the model parameters as derived in this work which might restrict such correction [37,38] not to exceed the Higgs mass.

As the purely triplet seesaw model [15,31] does not have dark matter prediction to explain observed relic density and mass bounds determined by direct and indirect detection experiments [39–43], it would enhance the model capabilities if the dark matter phenomena can be accommodated in its simple minimal extension as suggested in this work.

Despite the presence of two heavy Higgs triplets, we note that the renormalisation group running renders the Higgs quartic coupling in the model [15,31] to acquire negative values in the interval $|\phi| = (5 \times 10^9 - 10^{13})$ GeV leading to vacuum instability [44,45]. Noting that it is a natural compulsion to guarantee vacuum stability of the scalar potential in any of the model applications such as neutrino masses, baryon asymmetry and dark matter, we have shown in this work how the minimally extended model with scalar singlet dark matter ensures such a stability.

Compared to earlier works on purely triplet seesaw ansatz [15,31], in this work we have fitted the most recent neutrino data [1–3] including θ_{23} in the second octant and large Dirac CP-phase ($\delta \simeq 214^\circ$). We have further exposed the success of the model potential to be compatible with recent cosmological bounds determined from Planck satellite data [5,28]. In our approach, the dominant of the two matrices being completely determined from neutrino data, provides known values of lepton flavour and number violating couplings occurring in the CP-asymmetry parameters. In addition, optimal or randomised phase differences between the elements of the

two matrices provide a rich structure for CP-asymmetry parameters for unflavoured and flavoured leptogenesis. Using our model CP-asymmetry inputs, we find solutions of Boltzmann equations successfully predicting baryon asymmetry of the Universe in the unflavoured as well as two-flavoured regimes.

Highlights of the present work are

- The two-Higgs triplet seesaw model [15] is found to fit the most recent neutrino data including θ_{23} in the second octant and large Dirac CP-phases for both normal ordering (NO) and inverted ordering (IO) of neutrino masses in concordance with cosmological bounds determined from Planck satellite measurements [5,28].
- The model ansatz for CP-asymmetry and solutions of Boltzmann equations are found to predict the observed value of baryon asymmetry of the Universe in the case of unflavoured (two-flavoured) leptogenesis for the lighter triplet mass values $M_{\Delta_2} \simeq \mathcal{O}(10^{12})$ GeV ($M_{\Delta_2} \simeq \mathcal{O}(10^{11})$ GeV) with corresponding values of lepton number violating coupling μ_{Δ_2} in each case.
- Whereas the original model [15] does not have dark matter (DM), a simple extension of the model is found to predict a real scalar singlet WIMP [46] dark matter [47] in agreement with observed relic density and direct detection measurements which set the lower bound $m_\xi = 750$ GeV.
- This real scalar DM is also found to remove the vacuum instability of the scalar potential existing in the original model.
- When the vacuum stability constraint is combined with those due to relic density and direct detection measurements, this real scalar singlet mass limit is pushed from $m_\xi = 750$ GeV to $m_\xi = 1.3$ GeV which is verifiable by ongoing experiments.
- Despite the two heavy triplet scalar masses, the model parameters are noted to satisfy fine-tuned conditions necessary for the radiative stability of the standard Higgs mass.
- Using the two-Higgs triplet model [15] and its further simple extension, we have thus successfully addressed four important issues confronting the standard model: neutrino masses and mixings within cosmological bound, baryon asymmetry of the universe, dark matter, and vacuum stability of the scalar potential. In addition, we have derived necessary constraint on the model parameters for the radiative stability of standard Higgs mass.

This paper is organised in the following manner. In Sec. 2 we discuss the triplet leptogenesis model [15]. In Sec. 3 we discuss how the current neutrino data is fitted by two-triplet generated type-II seesaw formula with NO or IO masses consistent with cosmological bound where we also derive possible values of the scalar triplet masses and trilinear couplings for leptogenesis. Prediction of baryon asymmetry with detailed numerical analyses supported by proper graphical representation is presented in Sec. 4. Its subsections deal with different regimes of leptogenesis taking into account various schemes to choose the data set for leptogenesis calculation. Extension of the model to accommodate dark matter is discussed in Sec. 5, Sec. 5.1, and Sec. 5.1.1. In Sec. 5.1.3 we discuss the issue of vacuum instability of the scalar potential and its resolution with a summary on DM investigation in Sec. 5.1.4. In Sec. 6 we discuss Higgs mass stability constraint on the model parameters. The work is summarised in Sec. 7. Explanation and definition of different functions and parameters associated with Boltzmann equations are given in Sec. A.1, Sec. A.2 and Sec. A.3 while renormalisation group equations for gauge, scalar and top-quark Yukawa couplings have been discussed in Sec. A.4 of the Appendix.

2. The two-triplet model

Whereas in majority of models the RHNs have been found instrumental in theories of neutrino masses and leptogenesis, along with type-II dominance seesaw ansatz for neutrino mass possible realisation of leptogenesis in two-triplet extensions of standard model has been proposed in [15] without any RHN.

In other triplet seesaw and leptogenesis models [19,31,33], heavy RHNs are needed for loop mediation even though the triplet in collaboration with SM Higgs doublet is capable of explaining neutrino masses. But this model [15] does not need any RHN to implement both the phenomena: neutrino mass and leptogenesis for successful prediction of baryon asymmetry of the Universe. The resulting scalar potential in this model has different terms depending upon the SM Higgs field values $\mu = |\phi|$ as discussed in Sec. 5. The charges of fermions and scalars have been also defined in Sec. 5 in Table 2. Thus, in addition to the usual SM interactions and their modifications, the nonstandard part of the Lagrangian that contributes to type-II seesaw and leptogenesis is

$$-\mathcal{L}_{ext} = \sum_{\alpha=1}^{2} \Big((D_\mu \vec{\Delta}_\alpha)^\dagger . (D^\mu \vec{\Delta}_\alpha) - M^2_{\Delta_\alpha} Tr(\Delta^\dagger_\alpha \Delta_\alpha) + [\frac{1}{2} y^{(\alpha)}_{ij} L_i^T C i\tau_2 \Delta_\alpha L_j - \mu_{\Delta_\alpha} \phi^T i\tau_2 \Delta_\alpha \phi + h.c.] \Big). \tag{4}$$

Here $i, j = 1, 2, 3$ denote the three lepton flavors represented by the lepton doublets L_i but $\alpha = 1, 2$ denote the two scalar triplets. M_{Δ_α} = mass of the triplet Δ_α, $y^{(\alpha)}_{ij}$ = Majorana coupling of Δ_α with L_i and L_j and μ_{Δ_α} = lepton-number violating trilinear coupling of Δ_α with standard Higgs doublet ϕ.

Defining the induced triplet VEVs $V_{L_\alpha} (\alpha = 1, 2)$

$$V_{L_\alpha} = \frac{\mu_{\Delta_\alpha} v^2}{2M^2_{\Delta_\alpha}}, \tag{5}$$

the formula for the light neutrino mass matrix m_ν is

$$\begin{aligned} m_\nu &= 2y^{(1)} V_{L_1} + 2y^{(2)} V_{L_2}, \\ &= y^{(1)} \frac{\mu_{\Delta_1} v^2}{M^2_{\Delta_1}} + y^{(2)} \frac{\mu_{\Delta_2} v^2}{M^2_{\Delta_2}} \\ &\equiv m^{(1)}_\nu + m^{(2)}_\nu. \end{aligned} \tag{6}$$

Here $v = 246$ GeV, the standard Higgs vacuum expectation value (VEV).

2.1. CP asymmetry

Now we discuss about the source of lepton number violation and generation of CP asymmetry. It is clear from the interaction lagrangian (eq. (4)) that lepton number violation (LNV) is possible due to the coexistence of the Higgs triplet-bilepton Yukawa matrix y along with the trilinear coupling $\mu_{\Delta_\alpha} (\alpha = 1, 2)$. Since heavy RHNs are absent in the theory, the entire CP asymmetry is created due to the decay of the heavy scalar triplets. In tree level the scalar triplets can decay to bi-leptons as well as two SM Higgs. The corresponding branching ratios of Δ_α decay to leptons and SM Higgs are respectively

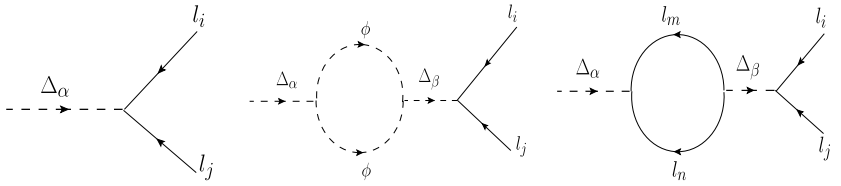

Fig. 1. Tree level and one loop Feynman diagrams for a triplet decaying to bi-leptons in case of flavoured leptogenesis.

$$B_l^\alpha = \sum_{i=e,\mu,\tau} B_{l_i}^\alpha = \sum_{i,j=e,\mu,\tau} B_{l_{ij}}^\alpha = \sum_{i,j=e,\mu,\tau} \frac{M_{\Delta_\alpha}}{8\pi\,\Gamma_{\Delta_\alpha}^{tot}} |y_{ij}^{(\alpha)}|^2 \text{ and} \tag{7}$$

$$B_\phi^\alpha = \frac{|\mu_{\Delta_\alpha}|^2}{8\pi\, M_\Delta \Gamma_{\Delta_\alpha}^{tot}}, \tag{8}$$

which obviously satisfy $B_l^\alpha + B_\phi^\alpha = 1$, where $\Gamma_{\Delta_\alpha}^{tot}$ is the total decay width of Δ_α, given by

$$\Gamma_{\Delta_\alpha}^{tot} = \frac{M_{\Delta_\alpha}}{8\pi}\Big(\sum_{i,j} |y_{ij}^{(\alpha)}|^2 + \frac{|\mu_{\Delta_\alpha}|^2}{M_{\Delta_\alpha}^2}\Big)\,. \tag{9}$$

The decay to bi-leptons can also occur due to one loop process where the loop is mediated by either SM Higgs or leptons as shown in Fig. 1.[1] The CP asymmetry arises due to the interference of the tree level contribution with that of the one loop wave function diagrams as shown in Fig. 1. Again the total flavoured CP asymmetry consists of two pieces, the scalar loop gives rise to a part which violates both lepton number and flavour whereas the one with lepton loop gives rise to only flavour violating asymmetry. So the total flavoured asymmetry (taking into account both lepton number + flavour violations, denoted by ($\not{L}, \not{F}$), and only lepton flavour violation denoted by $\not{F}$) is given by

$$\epsilon_{\Delta_\alpha}^{l_i} = \epsilon_{\Delta_\alpha}^{l_i(\not{L},\not{F})} + \epsilon_{\Delta_\alpha}^{l_i(\not{F})}\,. \tag{10}$$

In the present work we have considered only two heavy triplets corresponding to $\alpha = 1, 2$. It is well known that lepton asymmetry will be produced mostly due to the decay of the lighter triplet which is Δ_2 in our case while the asymmetry due to the heavier one will be washed out. Dynamical origin of neutrino masses is thus made consistent with the dominance of the Δ_2 to neutrino mass matrix over Δ_1. Therefore, in all the future expressions of CP asymmetries, branching ratios, decay widths we will omit the index on the scalar triplet. It is to be understood that $\epsilon_\Delta \equiv \epsilon_{\Delta_2}$, $B_l \equiv B_l^2$, $B_\phi \equiv B_\phi^2$. The above mentioned two pieces of CP asymmetry in eq. (10) arising due to Δ_2 decay are given by

$$\epsilon_\Delta^{l_i(\not{L},\not{F})} = \frac{1}{2\pi}\frac{Im\left\{\sum_n \left(y^{(2)}\right)_{ni}^* \left(y^{(1)}\right)_{ni} \mu_{\Delta_2}^* \mu_{\Delta_1}\right\}}{M_{\Delta_2}^2 Tr(y^{(2)} {y^{(2)}}^\dagger) + |\mu_{\Delta_2}|^2} g(x_{12}), \tag{11}$$

$$\epsilon_\Delta^{l_i(\not{F})} = \frac{1}{2\pi}\frac{Im\left\{({y^{(2)}}^\dagger y^{(1)})_{ii} Tr(y^{(2)} {y^{(1)}}^\dagger)\right\}}{M_{\Delta_2}^2 Tr(y^{(2)} {y^{(2)}}^\dagger) + |\mu_{\Delta_2}|^2} g(x_{12}), \tag{12}$$

[1] It is to be noted that we wish to study the leptogenesis phenomena in both the regimes above and below 10^{12} GeV. Lepton flavours become distinguishable below 10^{12} GeV. The resulting leptogenesis is termed as flavoured leptogenesis. Thus in the Feynman diagram we have denoted the lepton flavors with different indices.

where

$$g(x_{\alpha\beta}) = \frac{x_{\alpha\beta}(1-x_{\alpha\beta})}{(1-x_{\alpha\beta})^2 + x_{\alpha\beta}y},$$
$$x_{\alpha\beta} = \frac{M^2_{\Delta_\alpha}}{M^2_{\Delta_\beta}},$$
$$y = \left(\frac{\Gamma^{tot}_{\Delta_\beta}}{M_{\Delta_\beta}}\right)^2. \tag{13}$$

The indices n, i in the above expressions of CP asymmetries stand for the lepton flavour indices (e, μ, τ). It can be easily understood that if we sum over the flavour indices, the second piece of the CP asymmetry which is solely due to flavour violation vanishes identically, i.e.

$$\sum_{i=e,\mu,\tau} \epsilon^{l_i(\not{l})}_{\Delta} = 0\,. \tag{14}$$

This CP asymmetry parameter survives only in the case of flavoured leptogenesis. Since this asymmetry does not involve any lepton number violation, some times it is called purely flavoured asymmetry and the corresponding leptogenesis scenario which is dominated by the flavour violating CP asymmetry ($\epsilon^{l_i(\not{l})}_{\Delta} \gg \epsilon^{l_i(\not{L},\not{l})}_{\Delta}$) is referred to as purely flavoured (PFL) leptogenesis. The condition to get PFL leptogenesis can be shown to be [31]

$$\mu^*_{\Delta_2}\mu_{\Delta_1} \ll M^2_{\Delta_2} Tr(y^{(2)}y^{(1)\dagger})\,. \tag{15}$$

Therefore, consistent with dominance of $m^{(2)}_\nu$ over $m^{(1)}_\nu$ and the condition that $M_{\Delta_2} < M_{\Delta_1} \simeq \mu_{\Delta_1}$, PFL is not always guaranteed in flavoured leptogenesis regime. During our actual numerical analysis of flavoured leptogenesis we will examine whether PFL is achievable in our case.

The following set of parameters have been used for the model predictions in [15]

$$y^{(1)}_{kl} = 0.1\ (k,l = 1,2,3),\ y^{(2)}_{33} = 1,\ |\mu_{\Delta_1}| = 10^{13}\ \text{GeV},$$
$$|\mu_{\Delta_2}| = 2\times 10^{12}\ \text{GeV},\ M_{\Delta_1} = 3\times 10^{13}\ \text{GeV},\ M_{\Delta_2} = 10^{13}\ \text{GeV}, \tag{16}$$

consistent with QD neutrino mass eigenvalues

$$m_1 \sim m_2 \sim m_3 \sim 1.2eV \tag{17}$$

This choice leads to an interesting prediction for observable neutrinoless double beta decay close to the current experimental limit [25]. KATRIN [30] experimental search program has recently set the neutrino mass limit to $m_0 \leq 1$ eV.

However, recent estimations derived from Planck satellite data appear to constrain the QD spectrum considerably [5,28] as stated through eq. (1) and eq. (2). In addition the recent neutrino data has revealed certain significant interesting changes over previous results with the atmospheric neutrino mixing angle in the second octant $\theta_{23} \geq 45°$ and the Dirac CP phase $\delta \simeq 214°$. Success of a class of type-II seesaw dominant models but with RHN loop mediated triplet leptogenesis has been investigated along with predictions of new CP-asymmetry formulas in concordance with the recent oscillation data [33] and cosmological bound [5]. It is thus quite important to examine whether purely triplet seesaw and leptogenesis predictions without RHNs

could be compatible with the recent data, cosmological bound [5], baryon asymmetry [5,28] and dark matter while ensuring vacuum stability of the scalar potential.
In order to fit the recent neutrino data by the present formulation, we use the approximation that the type-II seesaw formula generated by lighter of the two triplets (with $M_{\Delta_2} \ll M_{\Delta_1}$) has dominant contribution, i.e.

$$m_\nu \simeq m_\nu^{(2)} = m_\nu^{(DATA)}. \tag{18}$$

$m_\nu^{(1)}$ and $m_\nu^{(2)}$ matrices can always be represented as

$$(m_\nu^{(1)})_{ij} = |m_\nu^{(1)}{}_{ij}| e^{i\phi_{ij}^{(1)}}, \ (m_\nu^{(2)})_{ij} = |m_\nu^{(2)}{}_{ij}| e^{i\phi_{ij}^{(2)}}, \tag{19}$$

which in turn gives

$$\frac{(m_\nu^{(1)})_{ij}}{(m_\nu^{(2)})_{ij}} = \frac{|m_\nu^{(1)}{}_{ij}|}{|m_\nu^{(1)}{}_{ij}|} e^{i(\phi_{ij}^{(1)} - \phi_{ij}^{(2)})}. \tag{20}$$

Under this assumption each element of $m_\nu^{(1)}$ is connected to the corresponding element of $m_\nu^{(2)}$ through a multiplicative factor which is a complex number in general and can be represented as

$$(m_\nu^{(1)})_{ij} = F_{ij} e^{i(\phi_{ij}^{(1)} - \phi_{ij}^{(2)})} (m_\nu^{(2)})_{ij} \tag{21}$$

where $F_{ij} = |m_\nu^{(1)}{}_{ij}|/|m_\nu^{(2)}{}_{ij}|$ which is a real ratio. In order to ensure the dominance of $m_\nu^{(2)}$ over $m_\nu^{(1)}$ we assume $F_{ij} \leq 0.1$ for all i, j. In general F_{ij}s and $(\phi_{ij}^{(1)} - \phi_{ij}^{(2)})$ can have different values for different combinations of i and j. Using eq. (6) and very near equality of $m_\nu^{(2)}$ with $m_\nu^{(DATA)}$, the numerical value of the Yukawa coupling matrix $y^{(2)}$ can be easily found for a known set of $(M_{\Delta_2}, \mu_{\Delta_2})$. Again for any random value of the ratio F_{ij} and the phase difference $(\phi_{ij}^{(1)} - \phi_{ij}^{(2)})$, the other Yukawa coupling $y^{(1)}$ can be computed from eq. (21) provided the corresponding trilinear coupling (μ_{Δ_1}) and the triplet mass (M_{Δ_1}) are already known. We may assume some numerical values $(M_{\Delta_2}, \mu_{\Delta_2})$ depending upon the regime of leptogenesis (flavoured/unflavoured) and then $(M_{\Delta_1}, \mu_{\Delta_1})$ can be accordingly chosen to keep $m_\nu^{(1)}$ sub-dominant, which in turn requires $M_{\Delta_1} \gg M_{\Delta_2}$. This also ensures the contribution of Δ_1 towards leptogenesis to be negligible. Knowledge of all these parameters along with some random value of the phase difference and the ratio enables us to calculate the flavoured CP asymmetry (eq. (11), (12)) parameters. However in the unflavoured regime the purely flavoured CP asymmetry part vanishes and we are left with (lepton number + flavour) violating part which can be represented in terms of the experimental value of light neutrino mass matrix (denoted as $m_\nu (= m_\nu^{\text{DATA}})$) as

$$\begin{aligned}
\epsilon_\Delta^l &= \sum_i \epsilon_\Delta^{l_i(\not{L},\not{F})} \\
&= \frac{M_{\Delta_1}^2 M_{\Delta_2}^2}{2\pi v^4} \frac{\sum_{ij} F_{ij} |(m_\nu)_{ij}|^2 \sin(\phi_{ij}^{(1)} - \phi_{ij}^{(2)})}{M_{\Delta_2}^2 Tr(y^{(2)} y^{(2)\dagger}) + |\mu_{\Delta_2}|^2} g(x_{12}) \qquad (22) \\
&\simeq \frac{M_{\Delta_1}^2 M_{\Delta_2}^2}{16\pi^2 v^4} \frac{\sum_{ij} F_{ij} |(m_\nu)_{ij}|^2 \sin(\phi_{ij}^{(1)} - \phi_{ij}^{(2)})}{(M_{\Delta_1}^2 - M_{\Delta_2}^2)} \left(\frac{M_{\Delta_2}}{\Gamma_{\Delta_2}^{tot}} \right). \qquad (23)
\end{aligned}$$

Then for $M_{\Delta_1} \gg M_{\Delta_2}$, the CP-asymmetry is

$$\epsilon^{l}_{\Delta} = \frac{M^2_{\Delta_2}}{16\pi^2 v^4} \sum_{ij} F_{ij} |(m_\nu)_{ij}|^2 \sin(\phi^{(1)}_{ij} - \phi^{(2)}_{ij}) \left(\frac{M_{\Delta_2}}{\Gamma^{tot}_{\Delta_2}}\right) . \tag{24}$$

2.2. Boltzmann equations for leptogenesis

Boltzmann equations are used to track the evolution of the particle asymmetries in the early universe where the hot plasma is composed of large number of particle species resulting in numerous reactions. However there is no need take into account all of them. Only those reactions are important whose rates at that temperature are comparable to the Hubble rate (i.e. $\Gamma(T) \sim H(T)$).

Lepton number violation is embedded in the interaction lagrangian (eq. (4)) through the Majorana type coupling of the triplet Higgs with bi-leptons. Lepton number is violated by two units whenever Δ decays to (l_i, l_j). As it is a baryon number conserving process, $(B-L)$ is also violated by two units. So our aim is to find out the evolution of abundance of $(B-L)$ which at later stage gets converted into baryon number through sphaleron transition process. It is worthwhile to mention that during the sphaleron process the quantity $(B-L)$ $(B/3-L_i)$ is conserved in case of unflavoured (flavoured) leptogenesis. Accordingly the asymmetry parameter whose evolution with temperature has to be traced is $(B-L)$ $((B/3-L_i))$ for unflavoured (flavoured) leptogenesis scenario. It is not possible to compute the evolution of $(B-L)$ or $(B/3-L_i)$ independently as it includes other parameters which also evolve with temperature. In fact the Boltzmann equations consist of a set of coupled differential equations which have to be solved simultaneously to find solution for any of the variables. In this purely triplet leptogenesis model the asymmetry can only be generated by the decay of heavy scalar triplet. Therefore, along with the first order differential of $(B-L)$ or $(B/3-L_i)$, the Boltzmann equations contain first order differentials of scalar triplet density and scalar triplet asymmetry. This scalar triplet asymmetry arises due to the fact that Δ_2 and $\Delta_2^\dagger$ are not self-conjugate. The right hand side of relevant Boltzmann equations contains interaction terms that tend to change the density of the corresponding variable. Considering all such interactions, the network of lepton flavour dependent coupled Boltzmann equations are [31–33]

$$\dot{Y}_\Sigma = -\Big(\frac{Y_\Sigma}{Y^{eq}_\Sigma} - 1\Big)\gamma_D - 2\Big[\Big(\frac{Y_\Sigma}{Y^{eq}_\Sigma}\Big)^2 - 1\Big]\gamma_A, \tag{25}$$

$$\dot{Y}_{\Delta_\Delta} = -\Big[\frac{Y_{\Delta_\Delta}}{Y^{eq}_\Sigma} - \sum_k \Big(\sum_i B_{l_i} C^l_{ik} - B_\phi C^\phi_k\Big)\frac{Y_{\Delta_k}}{Y^{eq}_l}\Big]\gamma_D, \tag{26}$$

$$\begin{aligned}\dot{Y}_{\Delta_{B/3-L_i}} = &-\Big[\Big(\frac{Y_\Sigma}{Y^{eq}_\Sigma} - 1\Big)\epsilon^{l_i}_\Delta - 2\sum_j \Big(\frac{Y_{\Delta_\Delta}}{Y^{eq}_\Sigma} - \frac{1}{2}\sum_k C^l_{ijk}\frac{Y_{\Delta_k}}{Y^{eq}_l}\Big)B_{l_{ij}}\Big]\gamma_D \\ &- 2\sum_{j,k}\Big(C^\phi_k + \frac{1}{2}C^l_{ijk}\Big)\frac{Y_{\Delta_k}}{Y^{eq}_l}\Big(\gamma^{\prime\phi\phi}_{l_i l_j} + \gamma^{\phi l_j}_{\phi l_i}\Big) \\ &- \sum_{j,m,n,k} C^l_{ijmnk}\frac{Y_{\Delta_k}}{Y^{eq}_l}\Big(\gamma^{\prime l_n l_m}_{l_i l_j} + \gamma^{l_m l_j}_{l_i l_n}\Big) \ . \end{aligned} \tag{27}$$

Notational conventions adopted here are as follows: Y_{Δ_X} stands for the ratio of number density (or difference of number density) to the entropy density, i.e. $Y_{\Delta_X} = \frac{n_X - n_{\bar{X}}}{s}$, where n_X $(n_{\bar{X}})$ is the X $(\bar{X})$ number density. Standard mathematical forms of equilibrium number densities of different particle species X $(\bar{X})$ are given in Sec. A.1 of Appendix. It is implied that the

variables of the differential equations ($Y_{\Delta_\Delta}, Y_\Sigma, Y_{\Delta_{B/3-L_i}}$) are function of $z = M_\Delta/T$. Here $\dot{Y}_X$ denotes $\dot{Y}_X \equiv \dot{Y}_X(z) = s(z)H(z)\frac{dY_X(z)}{dz}$. The scalar triplet density and asymmetry are denoted as $\Sigma = \Delta + \Delta^\dagger$ and $\Delta_\Delta = \Delta - \Delta^\dagger$, respectively. Superscript 'eq' denotes the equilibrium value of the corresponding quantity. Functional forms of all such equilibrium densities are presented in Sec. A.1 of Appendix. The total reaction density of the triplet including its decay and inverse decay to lepton pair or scalars is represented as γ_D. The gauge induced $2 \leftrightarrow 2$ scattering of triplets to fermions, scalars and gauge bosons is denoted by γ_A. Lepton flavour and number ($(\Delta L = 2)$) violating Yukawa scalar induced s channel ($\phi\phi \leftrightarrow \bar{l}_i\bar{l}_j$) and t channel ($\phi l_j \leftrightarrow \bar{\phi}\bar{l}_i$) scattering related reaction densities are denoted as $\gamma^{\phi\phi}_{l_i l_j}$ and $\gamma^{\phi l_j}_{\phi l_i}$, respectively. Similarly reaction densities related to Yukawa induced triplet mediated lepton flavour violating $2 \leftrightarrow 2$ s channel and t channel processes are denoted by $\gamma^{l_n l_m}_{l_i l_j}$ and $\gamma^{l_j l_m}_{l_i l_n}$. The primed s channel reaction densities are given by $\gamma' = \gamma - \gamma^{\text{on shell}}$. We present the explicit expressions of these reaction densities in Sec. A.2 of Appendix. The asymmetry coupling matrices C^l_{ijk} and C^l_{ijmnk} are defined as [31]

$$\begin{aligned} C^l_{ijk} &= C^l_{ik} + C^l_{jk}, \\ C^l_{ijmnk} &= C^l_{ik} + C^l_{jk} - C^l_{mk} - C^l_{nk}, \end{aligned} \tag{28}$$

where C^l matrix connects the asymmetry of lepton doublets with that of $B/3 - L_i$ whereas C^ϕ establishes a relation between the asymmetry of scalar triplet and $B/3 - L_i$, i.e.,

$$\begin{aligned} Y_{\Delta_{l_i}} &= -\sum_k C^l_{ik} Y_{\Delta_k} \\ Y_{\Delta_\phi} &= -\sum_k C^\phi_k Y_{\Delta_k} \end{aligned} \tag{29}$$

where Y_{Δ_k} represents the components of the asymmetry vector $\vec{Y}_\Delta$,

$$\vec{Y}_\Delta \equiv (Y_{\Delta_\Delta}, Y_{\Delta B/3-L_k})^T. \tag{30}$$

The generation index k in the above equation runs from 1 to 3 for fully (three) flavoured leptogenesis whereas it takes values 1, 2 for two flavoured leptogenesis which dictates the corresponding $\vec{Y}_\Delta$ will be a column matrix with four or three entries, respectively. C^l and C^ϕ matrices are determined from chemical equilibrium conditions. Their detailed structure and dimensionality in different temperature regimes are given in Sec. A.3 of Appendix. The flavoured Boltzmann equations presented in eqs. (25), (26), (27) have to be solved simultaneously upto a large value of z (where the asymmetry gets frozen). Then the final value of Baryon asymmetry parameter is computed to be

$$Y_B \equiv Y_{\Delta_B} = 3 \times \frac{12}{37} \sum_i Y_{\Delta_{B/3-L_i}} \tag{31}$$

where the factor 3 takes care of different $SU(2)$ degrees of freedom of the scalar triplet. When the mass of the decaying heavy particle (or equivalently the temperature for asymmetry generation) exceeds 10^{12} GeV, the charged lepton Yukawa interactions go out of equilibrium and, as a result, the lepton flavours lose their distinguishability. Thus we need not treat the flavours separately and as a result corresponding Boltzmann equations are free of lepton flavour index. This variant of leptogenesis is referred to as the unflavoured leptogenesis and the set of Boltzmann equations applicable to this case are obtained through modifications of eq. (25)–(27) [31] as

$$\dot{Y}_{\Sigma} = -\Big(\frac{Y_{\Sigma}}{Y_{\Sigma}^{eq}} - 1\Big)\gamma_D - 2\Big[\Big(\frac{Y_{\Sigma}}{Y_{\Sigma}^{eq}}\Big)^2 - 1\Big]\gamma_A \tag{32}$$

$$\dot{Y}_{\Delta_{\Delta}} = \Big[\frac{Y_{\Delta_{\Delta}}}{Y_{\Sigma}^{eq}} - \sum_k \Big(B_l C_k^l - B_{\phi} C_k^{\phi}\Big)\frac{Y_{\Delta_k}}{Y_l^{eq}}\Big]\gamma_D, \tag{33}$$

$$\begin{aligned}\dot{Y}_{\Delta_{B-L}} = &-\Big[\Big(\frac{Y_{\Sigma}}{Y_{\Sigma}^{eq}} - 1\Big)\epsilon_{\Delta}^l - 2\Big(\frac{Y_{\Delta_{\Delta}}}{Y_{\Sigma}^{eq}} - \sum_k C_k^l \frac{Y_{\Delta_k}}{Y_l^{eq}}\Big)B_l\Big]\gamma_D \\ &- 2\sum_k \Big(C_k^{\phi} + C_k^l\Big)\frac{Y_{\Delta_k}}{Y_l^{eq}}\Big(\gamma_{ll}^{\prime\phi\phi} + \gamma_{\phi l}^{\phi l}\Big),\end{aligned} \tag{34}$$

where ϵ_{Δ}^l $(= \sum_i \epsilon_{\Delta}^{l_i})$ is the flavor summed or unflavoured CP asymmetry parameter and the asymmetry vector $\vec{Y}_{\Delta}$ has now been reduced to a column vector with only two entries, $\vec{Y}_{\Delta}^T = (Y_{\Delta_{\Delta}}, Y_{\Delta_{B-L}})$. Thus, in this case too, the final baryon asymmetry is computed using the simple formula of eq. (31) where the whole quantity under the summation should be replaced by a single asymmetry parameter $Y_{\Delta_{B-L}}$.

2.3. Flavour decoherence and different regimes of leptogenesis

Whether the lepton flavours have to be treated separately at a certain temperature is decided completely by the phenomenon of flavour decoherence [31]. It is a common practice to assume that flavour decoherence sets in as soon as the corresponding charged lepton Yukawa interaction rate exceeds the Hubble rate at that very temperature. Along with this assumption, few intricate details of the underlying processes are also taken into account to deal with this flavour decoherence issue. In the present model under consideration (SM + two triplets Δ_1, Δ_2) with $\Delta_2 \equiv \Delta$ and $M_{\Delta} < M_{\Delta_1}$, it is logical to assume survival of leptogenesis caused by the Δ decay. Then the flavour decoherence is dictated by the competition of two processes: SM charged lepton Yukawa interaction and inverse decay of leptons to triplet Δ. To clarify this statement let us assume that at some temperature (T_h) during the evolution of Universe, the charged lepton Yukawa interaction is faster than the Hubble rate but slower compared to triplet inverse decay ($ll \to \bar{\Delta}$). As a result the charged leptons inverse decay before the triplet can undergo any charged lepton Yukawa interaction. Even then it is still impossible to differentiate between the lepton flavours. At some later stage of evolution when the temperature of the thermal bath becomes lower, the charged leptons inverse decay rate by virtue of being Boltzmann suppressed gets reduced further. Then, at a temperature $T = T_{decoh}$, when the lepton inverse decay rate to $\bar{\Delta}$ becomes less than the lepton Yukawa interaction rate, the decoherence between the lepton flavours is achieved. Thus, between the temperature range $(T_h - T_{decoh})$, the flavour decoherence is not fully achieved, i.e. within this intermediate temperature regime, it is not totally justified to use flavoured leptogenesis formalism.

The decoherence temperature (T_{decoh}) is determined by the mass of the lighter of the two scalar triplets ($M_{\Delta} (= M_{\Delta_2})$) and the effective decay parameter [31]

$$\tilde{M}_{\Delta}^{eff} = \tilde{M}_{\Delta}\sqrt{\frac{1 - B_{\phi}}{B_{\phi}}}, \tag{35}$$

where

$$\tilde{M}_{\Delta}^{2} = |\mu_{\Delta}|^{2} \frac{v^{4}}{M_{\Delta}^{4}} Tr[YY^{\dagger}], \tag{36}$$

and B_{ϕ} is branching ratio of $\Delta \to \phi\phi$.

Decoherence is fully achieved when our chosen parameter space satisfies the condition that, at a given temperature, lepton triplet inverse decay rate is slower than the SM charged lepton Yukawa interaction rate. Imposition of this condition will lead us to an upper limit on M_{Δ} as a function of $\tilde{M}_{\Delta}^{eff}$ which can be expressed as

$$\Gamma_{f_i} \geq B_l \Gamma_{\Delta}^{tot} \frac{Y_{\Sigma}^{eq}}{Y_{l}^{eq}} \quad (\text{with } f_i = \tau, \mu). \tag{37}$$

Here B_l is the branching ratio of dilepton decay rate $\Delta_2 \to ll$ that occurs due to Yukawa interaction. This constraint relation can be translated into constraints over M_{Δ} and $\tilde{M}_{\Delta}^{eff}$ as [31]

$$M_{\Delta} \leq 4 \times \left(\frac{10^{-3}\ \text{eV}}{\tilde{M}_{\Delta}^{eff}}\right) \times 10^{11}\ \text{GeV} \quad (\text{fully two flavoured}), \tag{38}$$

$$M_{\Delta} \leq 1 \times \left(\frac{10^{-3}\ \text{eV}}{\tilde{M}_{\Delta}^{eff}}\right) \times 10^{9}\ \text{GeV} \quad (\text{fully three flavoured})\ . \tag{39}$$

Following eq. (38) and eq. (39) we can say that, when the mass of the decaying triplet $M_{\Delta} > 4 \times 10^{11}$ GeV, all the lepton flavours act as a coherent superposition and the corresponding asymmetry generation proceeds through unflavoured or single flavoured leptogenesis. When the temperature (or equivalently M_{Δ}) drops below 4×10^{11} GeV, the τ flavour gets decoupled whereas $e + \mu$ still act indistinguishably. Thus, the coherent superposition is effectively split into two flavours ($e + \mu$ and τ) and the corresponding leptogenesis phenomena is termed as 2-flavoured (or τ-flavoured) leptogenesis. Below 10^{9} GeV, all the charged lepton Yukawa interactions reach equilibrium and flavour decoherence is fully attained resulting in 3-flavoured (or fully flavoured) leptogenesis.

3. Model fitting of neutrino data within cosmological bound

In this section at first we discuss the model capability to fit the most recent neutrino data satisfying the constraint imposed by cosmological bounds [5,28]. Using the PDG convention [48] we parameterize the PMNS mixing matrix

$$U_{\text{PMNS}} = \begin{pmatrix} c_{12}c_{13} & s_{12}c_{13} & s_{13}e^{-i\delta} \\ -s_{12}c_{23} - c_{12}s_{23}s_{13}e^{i\delta} & c_{12}c_{23} - s_{12}s_{23}s_{13}e^{i\delta} & s_{23}c_{13} \\ s_{12}s_{23} - c_{12}c_{23}s_{13}e^{i\delta} & -c_{12}s_{23} - s_{12}c_{23}s_{13}e^{i\delta} & c_{23}c_{13} \end{pmatrix} diag(e^{\frac{i\alpha_M}{2}}, e^{\frac{i\beta_M}{2}}, 1) \tag{40}$$

where $s_{ij} = \sin\theta_{ij}, c_{ij} = \cos\theta_{ij}$ with $(i, j = 1, 2, 3)$, δ is the Dirac CP phase and (α_M, β_M) are Majorana phases. We use the best fit values of the oscillation data [2,3] as summarised below in Table 1.

Important among new interesting salient features of this set of data points are: (i) the best fit value of atmospheric mixing angle θ_{23} is in the second octant, (ii) large values of Dirac CP phases exceeding $\delta = 200^{\circ}$. The data Table 1 includes the reactor neutrino mixing $\theta_{13} = 8.6^{\circ}$ which was known earlier.

Table 1
Input data from neutrino oscillation experiments [2,3].

Quantity	Best fit values	3σ ranges
Δm^2_{21} [10^{-5} eV^2]	7.39	$6.79 - 8.01$
$\lvert\Delta m^2_{31}\rvert$ [10^{-3} eV^2] (NO)	2.52	$2.427 - 2.625$
$\lvert\Delta m^2_{32}\rvert$ [10^{-3} eV^2] (IO)	2.51	$2.412 - 2.611$
$\theta_{12}/^\circ$	33.82	$31.61 - 36.27$
$\theta_{23}/^\circ$ (NO)	49.6	$40.3 - 52.4$
$\theta_{23}/^\circ$ (IO)	49.8	$40.6 - 52.5$
$\theta_{13}/^\circ$ (NO)	8.61	$8.22 - 8.99$
$\theta_{13}/^\circ$ (IO)	8.65	$8.27 - 9.03$
$\delta/^\circ$ (NO)	215	$125 - 392$
$\delta/^\circ$ (IO)	284	$196 - 360$

Using the mass-squared differences from Table 1 and choosing the lightest mass eigenvalue $m_1 = 0.001$ eV, we at first determine the other two mass eigenvalues. Then using the three mass eigenvalues, mixing angles and phases given in Table 1 we derive neutrino mass matrix consistent with best fit to the data through the standard relation

$$m_\nu = U_{PMNS}\, diag(m_1, m_2, m_3) U^T_{PMNS}\,. \tag{41}$$

For NO and IO cases we get the following results:

Normal ordering (NO):

$$m_1 = 0.001 \text{ eV},\ m_2 = 0.0086 \text{ eV},\ m_3 = 0.0502 \text{ eV},$$
$$\sum_i m_i = 0.0598 \text{ eV} \ll \Sigma_{Planck},\ \text{or}\ \Sigma_{new} \tag{42}$$

where $\Sigma_{Planck} = 0.23$ eV of eq. (1) and $\Sigma_{new} = 0.12$ eV of eq. (2) are cosmological bounds derived in [5] and [28], respectively, using the Planck satellite data and the ΛCDM big-bang cosmological model of the Universe. We thus find that our best fit of the present neutrino data easily satisfies both the cosmological bounds in the NO case. We have noted [49] that within the 3σ uncertainty, the oscillation data can accommodate lower (higher) values of $\sum_i m_i$ with $m_1 < 0.001$ eV (0.001 eV $< m_1 \leq 0.04$ eV) consistent with the cosmological bound Σ_{Planck} [5]. But when $m_1 > 0.04$ eV, the bound Σ_{new} [28] is violated. For best fit values of masses, the neutrino mass matrix constructed from neutrino data is

$$m_\nu^{\rm NO}(\text{eV}) = \begin{pmatrix} 0.00367 - 0.00105i & -0.00205 + 0.00346i & -0.00634 + 0.00294i \\ -0.00205 + 0.00346i & 0.03154 + 0.00034i & 0.02106 - 0.0001i \\ -0.00634 + 0.00294i & 0.02106 - 0.0001i & 0.02383 - 0.00027i \end{pmatrix}. \tag{43}$$

This gives

$$\sum_{n,l} |m^{\rm NO}_{\nu,nl}|^2 = 2.595 \times 10^{-3} \text{ eV}^2\,. \tag{44}$$

Its close vicinity with Δm^2_{31} value of Table 1 in the NO case is noteworthy.

Although here we have presented the numerical values of $(m_\nu)_{ij}$ only for the best fit of neutrino oscillation data, the analysis can be easily extended for 3σ range of the extant data. We have to start with a suitably chosen value of the lightest eigenvalue (m_1). Then the 3σ range of solar (Δm^2_{21}) and atmospheric (Δm^2_{31}) mass squared differences provides a range of values for $m_2(=\sqrt{m_1^2+\Delta m^2_{21}})$ and $m_3(=\sqrt{m_1^2+\Delta m^2_{31}})$ such that the set (m_1, m_2, m_3) remains compatible with the 3σ limit. Plugging in these mass eigenvalues along with all possible combinations and the mixing angles within the 3σ uncertainty of oscillation data as presented in the third column of Table 1 in eq. (41), we can generate large number of sets of m_ν matrix. It is easy to realise that elements of the resulting m_ν matrix are constrained to vary within a range as dictated by the 3σ uncertainty of the oscillation data. Since we are dealing with purely triplet seesaw, the Yukawa coupling matrix ($= y^{(2)}$) has one-to-one correspondence with m_ν. Elements of m_ν and $y^{(2)}$ differ only by a scale factor $(\mu_{\Delta_2} v^2/M^2_{\Delta_2})$. A detailed analysis on 3σ and 1σ fit of neutrino oscillation data (including both NO and IO) for Type-II seesaw has already been presented in our previous work [49]. Therefore we are not repeating the whole analysis here.

Inverted ordering (IO):

$$\begin{aligned} &m_1 = 0.04938 \text{ eV},\ m_2 = 0.0501 \text{ eV},\ m_3 = 0.001 \text{ eV},\\ &\sum_i m_i = 0.100 \text{ eV} < \Sigma_{Planck},\ \text{or}\ \Sigma_{new}, \end{aligned} \tag{45}$$

where $\Sigma_{Planck} = 0.23$ eV [5] and $\Sigma_{new} = 0.12$ eV [28] given in eq. (1) and eq. (2), respectively. Both the bounds have been derived using Planck satellite data [28]. It is clear that the best fit in the IO case also satisfies both the cosmological bounds.

$$m_\nu^{IO}(\text{eV}) = \begin{pmatrix} 0.0484 - 0.00001i & -0.001122 + 0.0055i & -0.00137 + 0.00471i \\ -0.001122 + 0.0055i & 0.02075 - 0.00025i & -0.02459 - 0.00026i \\ -0.00137 + 0.00471i & -0.02459 - 0.00026i & 0.02910 - 0.00026i \end{pmatrix}. \tag{46}$$

The manifestly hierarchical nature of mass eigenvalues are evident from eq. (42) and eq. (45). This gives

$$\sum_{n,l} |m^{\text{IO}}_{\nu,nl}|^2 = 4.9 \times 10^{-3} \text{ eV}^2 \tag{47}$$

which is nearly 2 times larger than the Δm^2_{32} value of Table 1 in the IO case. In both the NO and IO cases, the sum of the three neutrino masses are also consistent with the upper bound $\Sigma_{new} = 0.12$ eV [28].

4. Estimation of baryon asymmetry

In general baryon asymmetry is expressed as excess of matter over anti-matter scaled by entropy density or photon density which, in practice, are expressed by two nearly equivalent quantities Y_B or η_B defined below, i.e.

$$Y_B = \frac{n_B - n_{\overline{B}}}{s}, \tag{48}$$

where $n_B, n_{\overline{B}}$ are number densities of baryons and anti-baryons, respectively, and s is the entropy density and

$$\eta_B = \frac{n_B - n_{\overline{B}}}{n_\gamma}, \tag{49}$$

where n_γ = photon density. Their values as observed by recent Planck satellite experiment [5] are

$$(\eta_B)_0 = (6 - 6.6) \times 10^{-10}, \tag{50}$$

or equivalently

$$(Y_B)_0 = (8.55 - 9.37) \times 10^{-11}, \tag{51}$$

where subscript zero indicates that the value of the corresponding asymmetry parameter is at the present epoch. In the present model under consideration the asymmetry is at first generated in the leptonic sector where lepton flavour and number violating decays of the heavy scalar triplet to bi-leptons gives rise to the lepton asymmetry which, later, gets converted into baryon asymmetry through sphaleron process. As we have clarified through an exhaustive discussion in Sec. 2.3 that, depending upon the mass of the decaying particle, the asymmetry production and its evolution down the temperature occur via unflavoured or flavoured leptogenesis. In the sections below we present a systematic and elaborate study of scalar triplet leptogenesis in unflavoured and flavoured regimes through support of proper numerical data with graphical analysis.

4.1. Unflavoured regime

In this regime the mass $M_{\Delta_2} = M_\Delta$ of the decaying particle $\Delta_2 (= \Delta)$, which is mainly responsible for asymmetry generation, is $M_\Delta \gtrsim 4 \times 10^{11}$ GeV. As discussed earlier, lepton flavours in this regime are indistinguishable and their coherent superposition acts as a single entity. Therefore, to calculate the baryon asymmetry, at first we have to compute the flavour summed CP asymmetry parameter ϵ^l_Δ given in eqs. (22), (23) which has to be plugged into the set of unflavoured Boltzmann equations (32)–(34). Simultaneous solution of those equations upto a large value of $z = M_\Delta / T$ (or equivalently low temperature) will provide us the freeze-in value of $(B - L)$ asymmetry. A fraction of this freeze-in value will be converted into baryon asymmetry (Y_B) through sphaleron process which is shown in eq. (31). Throughout the analysis we use a fixed set of values for the heavier triplet mass and its associated tri-linear coupling $M_{\Delta_1} = 3 \times 10^{13}$, $\mu_{\Delta_1} = 10^{13}$ (GeV). For the phase differences between the corresponding elements of $m_\nu^{(1)}$ and $m_\nu^{(2)}$ we follow two conventions for our numerical computations: (i) Fixed phase differences for all the elements, (ii) Random and different values of phase differences. Numerical results using both these conventions are discussed in the following two subsections.

4.1.1. Identical mass ratio and fixed phase difference connecting $m_\nu^{(1)}$ and $m_\nu^{(2)}$

As we can see from the expression of the unflavoured CP asymmetry parameter (eq. (23)) two very important ingredients in its calculation are the modulus ratio (F_{ij}) and phase difference $(\phi_{ij}^{(1)} - \phi_{ij}^{(2)})$ between the corresponding elements of $m_\nu^{(1)}$ and $m_\nu^{(2)}$. In this section our numerical results will be limited to the first convention with a fixed choice of ratio and phase differences which are again identical for all the elements, i.e. we use $F_{ij} = 0.1$ and $(\phi_{ij}^{(1)} - \phi_{ij}^{(2)}) = -\pi/2$ for all i, j. For numerical value of $(m_\nu)_{ij}$ we use best fit values of the neutrino oscillation observables in normal mass ordering (NO) as presented in eq. (43). We proceed to calculate the baryon asymmetry for two benchmark values of the lighter triplet mass ($M_{\Delta_2} = 5 \times 10^{11}, 10^{12}$ GeV) in the unflavoured regime. For each of the fixed benchmark value of M_{Δ_2} the corresponding

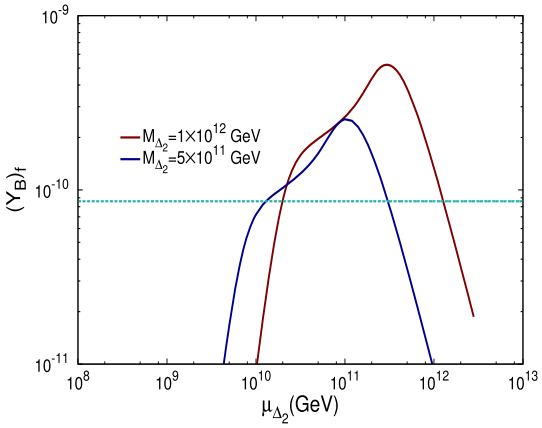

Fig. 2. Variation of final value of baryon asymmetry with trilinear coupling for two fixed benchmark values of lighter triplet mass using best fit values of NO type neutrino masses. The horizontal dashed line represents the experimental value of baryon asymmetry.

trilinear coupling μ_{Δ_2} is varied over a large range and for each combination of $(M_{\Delta_2}, \mu_{\Delta_2})$ final value of baryon asymmetry (Y_B) is evaluated. The variation of final Y_B, denoted by $(Y_B)_f$ in the figure, with μ_{Δ_2} for these two fixed values of M_{Δ_2} is shown graphically in Fig. 2. The dashed line intersects the $(Y_B)_f$ vs μ_{Δ_2} curve in two places which signifies that for fixed value of M_{Δ_2} there are two μ_{Δ_2} values which can produce baryon asymmetry within the experimental range. We now choose one such combination $(M_{\Delta_2} = 10^{12}, \mu_{\Delta_2} = 2 \times 10^{10}$ GeV)[2] from the Fig. 2 and show the evolution of different variables of the Boltzmann equation with z in Fig. 3. From the right panel of Fig. 3 it is clear that the final value of Y_B indeed freezes to $\sim 8.6 \times 10^{-11}$ (which is well inside the range (eq. (51)) as observed by the Planck satellite experiment).

For the sake of completeness we have repeated the same analysis using IO for light neutrino masses i.e. every other parameters remains the same except for $(m_\nu)_{ij}$ we use eq. (46). The resulting plot for the final values of Y_B with μ_{Δ_2} is presented in Fig. 4. It gives similar plot as that of the NO case, the only difference is that for a fixed M_{Δ_2} the value of μ_{Δ_2} required to produce same Y_B is shifted slightly to a higher value. Again the evolution of different variables of the Boltzmann equation with z (for the fixed set $(M_{\Delta_2} = 10^{12}, \mu_{\Delta_2} = 2.4 \times 10^{10}$ GeV)) is shown in Fig. 5.

In a simplistic approach if we neglect the triplet asymmetry term (Y_{Δ_Δ}) then we are left with only two coupled differential equations involving Y_Σ and Y_{B-L}. Again in case of very weak washout, the wash-out term can be neglected, i.e. the 2nd Boltzmann equation contains only the source term. This assumption lead us to a set of Boltzmann equations which are same as those presented in [15], i.e.

$$\dot{Y}_\Sigma = -\Big(\frac{Y_\Sigma}{Y_\Sigma^{eq}} - 1\Big)\gamma_D - 2\Big[\Big(\frac{Y_\Sigma}{Y_\Sigma^{eq}}\Big)^2 - 1\Big]\gamma_A \tag{52}$$

[2] Although we are showing graphical representation of solution of Boltzmann equation only for this combination, rigorous solution of the Boltzmann equation has been carried out for each and every combinations of $(M_{\Delta_2}, \mu_{\Delta_2})$ shown in Fig. 2.

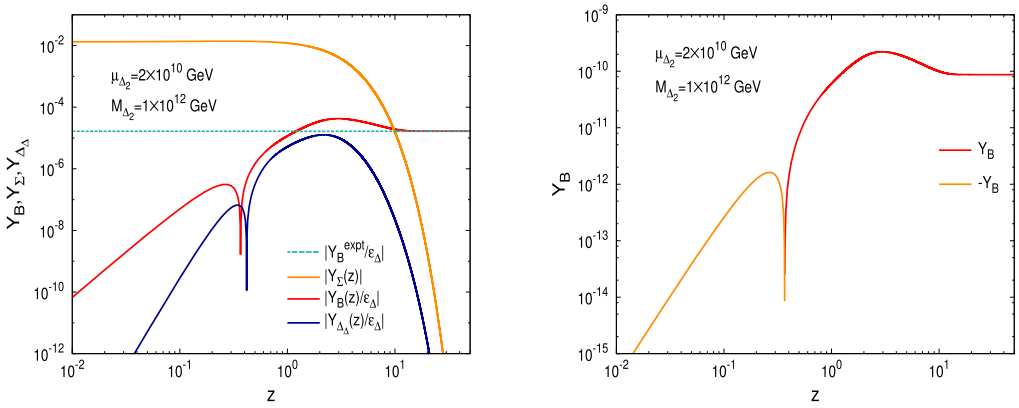

Fig. 3. Left panel: Evolution of different variables of the Boltzmann equation with $z = M_{\Delta_2}/T$ for the fixed set ($M_{\Delta_2} = 10^{12}, \mu_{\Delta_2} = 2 \times 10^{10}$ GeV) and best fit to oscillation data with NO type neutrino masses. The horizontal dashed line represents the experimental value of baryon asymmetry. Y_B and Y_{Δ_Δ} are scaled by the modulus value of unflavoured CP asymmetry parameter denoted by ε_Δ in the plot; Right panel: variation of Y_B with z for the same fixed set of $(M_{\Delta_2}, \mu_{\Delta_2})$.

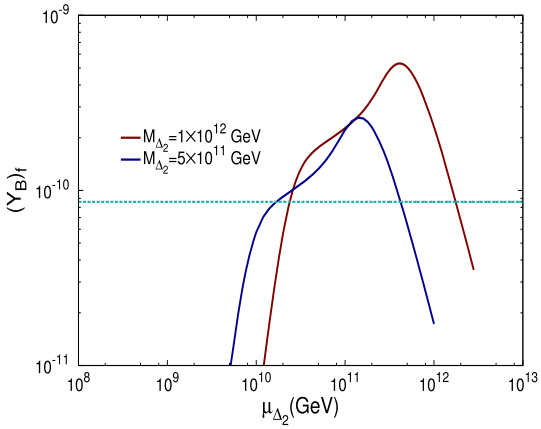

Fig. 4. Variation of final value of baryon asymmetry with trilinear coupling for two fixed benchmark values of lighter triplet mass M_{Δ_2} and IO type light neutrino masses. The horizontal dashed line represents the experimental value of baryon asymmetry.

$$\dot{Y}_{\Delta_{B-L}} = -\Big(\frac{Y_\Sigma}{Y_\Sigma^{eq}} - 1\Big)\epsilon_\Delta^l \,. \tag{53}$$

Proceeding exactly in a similar manner we compute final Y_B through solution of these two equations for two benchmark values of M_{Δ_2} whereas μ_{Δ_2} is varied over a wide range of values. The resulting plot of final Y_B with μ_{Δ_2} is presented below in Fig. 6 for both the NO and IO type neutrino mass orderings. Due to the absence of the washout term the asymmetry produced in this case (for a fixed set of $(M_{\Delta_2}, \mu_{\Delta_2})$) is much higher than the value given by solution of the full set of Boltzmann equations (Fig. 2, Fig. 4). The triplet asymmetry which has been omitted in this treatment has a non-trivial effect and also neglecting the washout term (without proper estimation of the decay parameter $(K = \Gamma_{\Delta_2}^{tot}/H)$) may lead to overestimation of the asymmetry.

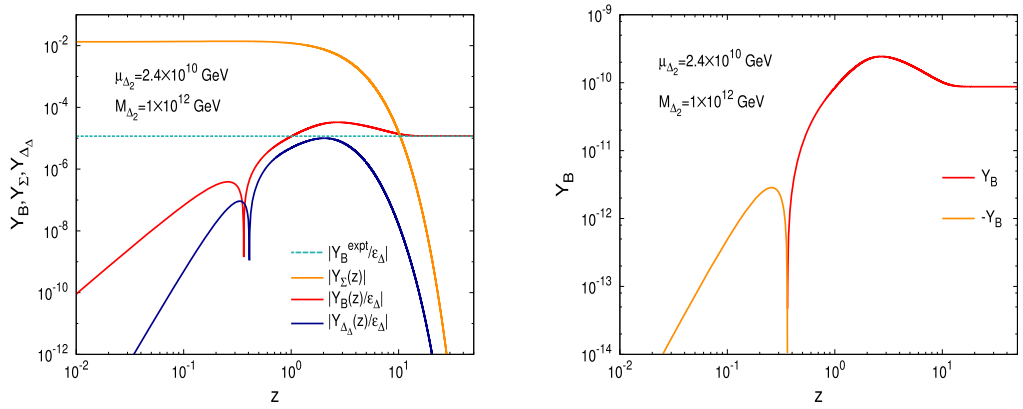

Fig. 5. Left panel: Evolution of different variables of the Boltzmann equation with z for the fixed set $(M_{\Delta_2} = 10^{12}, \mu_{\Delta_2} = 2.4 \times 10^{10}$ GeV) for best fit to oscillation data with IO type neutrino masses. The horizontal dashed line represents the experimental value of baryon asymmetry. Y_B and Y_{Δ_Δ} are scaled by the modulus value of unflavoured CP asymmetry parameter denoted by ε_Δ in the plot; Right panel: variation of Y_B with z for the same fixed set of $(M_{\Delta_2}, \mu_{\Delta_2})$.

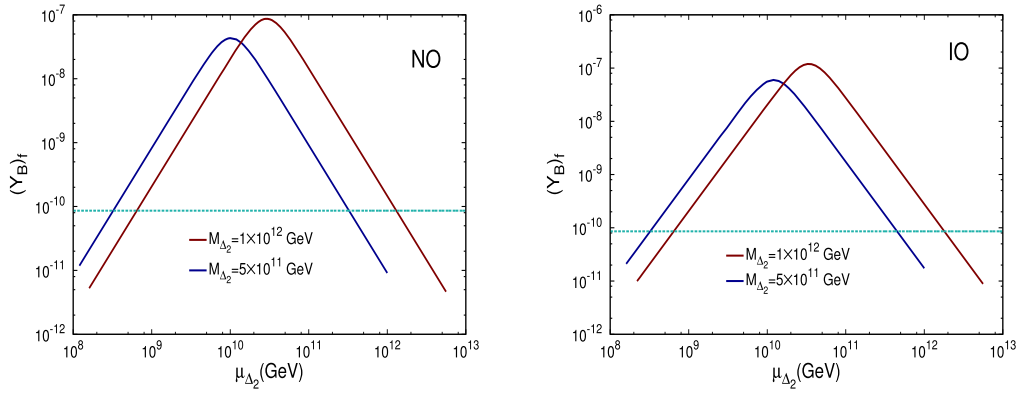

Fig. 6. Variation of baryon asymmetry with trilinear coupling for two fixed benchmark values of lighter triplet mass neglecting triplet asymmetry and washout. The horizontal dashed line represents the experimental value of baryon asymmetry. The left-panel (right-panel) represents solutions for NO (IO) type light neutrino mass hierarchy.

We present this analysis just for comparison. For all the future studies in this work we will use the full set of Boltzmann equations.

It is worthwhile to mention that pattern of the $(Y_B)_f$ vs μ_{Δ_2} plot exactly follows the variation of the CP asymmetry (ϵ^l_Δ) with μ_{Δ_2}. In our analysis all the parameters except the trilinear coupling (μ_{Δ_2}) are fixed. In the expression of CP asymmetry parameter ϵ^l_Δ (eq. (22)), μ_{Δ_2} dependence is contained only in the total triplet decay width $(\Gamma^{tot}_{\Delta_2})$, and $\epsilon^l_\Delta(|\mu_{\Delta_2}|) \sim 1/\Gamma^{tot}_{\Delta_2}(|\mu_{\Delta_2}|)$ where

$$\Gamma^{tot}_{\Delta_2}(|\mu_{\Delta_2}|) = c_1|\mu_{\Delta_2}|^2 + \frac{c_2}{|\mu_{\Delta_2}|^2}, \tag{54}$$

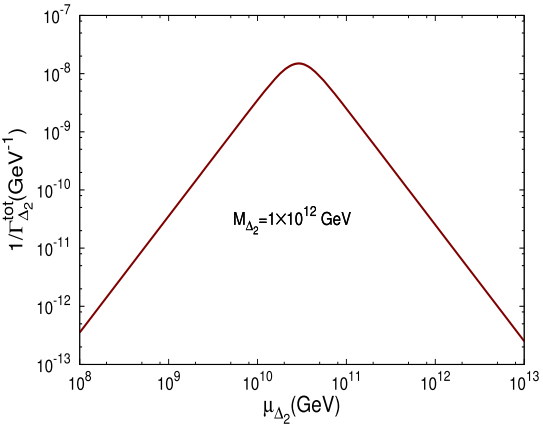

Fig. 7. Dependence of total decay width $\Gamma^{tot}_{\Delta_2}$ (of the lighter triplet) on the trilinear coupling μ_{Δ_2} for fixed a mass of the scalar triplet Δ_2 taking NO for light neutrinos and best fit values of the oscillation data.

with $c_1 = \frac{1}{8\pi M_{\Delta_2}}$ and $c_2 = \frac{M^5_{\Delta_2} Tr\left(m_\nu m_\nu^\dagger\right)}{8\pi v^4}$. In the plot (Fig. 7) below we depict the μ_{Δ_2} dependence of $1/\Gamma^{tot}_{\Delta_2}$ which shows a peak near[3] $\mu_{\Delta_2} = \left(\frac{c_2}{c_1}\right)^{1/4}$. It is obvious that the CP asymmetry will exactly follow this pattern and the final baryon asymmetry which is also directly proportional to CP asymmetry will also closely follow the same type of μ_{Δ_2} dependence.

4.1.2. Identical mass ratio but random phase differences connecting $m_\nu^{(1)}$ and $m_\nu^{(2)}$

We denote the phase difference between two corresponding elements of $m_\nu^{(1)}$ and $m_\nu^{(2)}$ as $\phi_{ij} = (\phi_{ij}^{(1)} - \phi_{ij}^{(2)})$. In the most general case, we need a set of six independent phase parameters $\{\phi_{11}, \phi_{12}, \phi_{13}, \phi_{22}, \phi_{23}, \phi_{33}\}$ and modulus ratios $\{F_{11}, F_{12}, F_{13}, F_{22}, F_{23}, F_{33}\}$ to connect $m_\nu^{(1)}$ and $m_\nu^{(2)}$ since they are both complex symmetric Majorana type matrices. We denote the set of phases and ratios as a whole by $\Phi_k \equiv \{\phi_{11}, \phi_{12}, \phi_{13}, \phi_{22}, \phi_{23}, \phi_{33}\}_k$ and $\mathcal{F}_k \equiv \{F_{11}, F_{12}, F_{13}, F_{22}, F_{23}, F_{33}\}_k$, where k denotes one of the sets. Here we generate a large number sets $\Phi_{k=1,...N}$ for the phase differences where each of the component phases is an absolute random number in the range $-\pi \leq \phi_{ij} \leq \pi$. But for the sake of simplicity we have limited ourselves to the case of identical modulus ratio for all the elements $(i, j = 1, 3)$, i.e. $\mathcal{F}_{k=1,....N} = \{0.1, 0.1, 0.1, 0.1, 0.1, 0.1\}$ for each and every sets marked as $k = 1, ..., N$. At first we estimate the unflavoured CP asymmetry parameter (ϵ^l_Δ) for the N number of random sets and then choose those sets among them which gives rise to negative value of the CP asymmetry parameter.[4] Naturally, imposition of this constraint ($\epsilon^l_\Delta < 0$ or equivalently $Y_B > 0$) reduces the number of allowed sets to $\sim N/2$. To get the value of final baryon asymmetry parameter (Y_B), the set of coupled Boltzmann equations, eq. (32)-eq. (34) have to be solved approximately $N/2$ times which is time consuming or rather repetitive. Therefore, we pick a random set

[3] Its numerical value is $\mu_{\Delta_2} = 2.9 \times 10^{10}$ GeV assuming NO, taking best fit values of oscillation data and triplet mass fixed at $M_{\Delta_2} = 10^{12}$ GeV.

[4] For the unflavoured leptogenesis case there is relative negative sign in the formula connecting CP asymmetry $((\epsilon^l_\Delta))$ and the final baryon asymmetry parameter (Y_B). Therefore to get positive Y_B, the CP asymmetry (ϵ^l_Δ) must be negative.

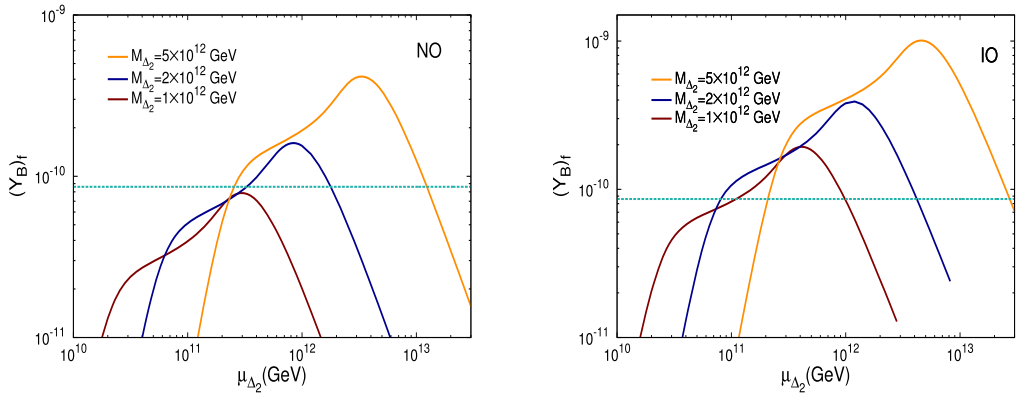

Fig. 8. Variation of baryon asymmetry with trilinear coupling μ_{Δ_2} for three fixed benchmark values of lighter triplet mass M_{Δ_2} derived by the solution full set of Boltzmann equations. The horizontal dashed line represents the experimental value of baryon asymmetry. The left-panel and the right-panel represent the result for NO and IO cases, respectively, consistent with the best fit to the oscillation data.

$$\frac{\Phi_{k=k_{random}}}{\pi} \equiv \{-0.3418, -0.0807, 0.7850, 0.9961, -0.4427, 0.7244\} \tag{55}$$

as a representative set among those $N/2$ and proceed further for the calculation of baryon asymmetry in NO and IO cases. In Fig. 8 we show the dependence of the final baryon asymmetry on the trilinear coupling μ_{Δ_2} for three benchmark values of the triplet mass M_{Δ_2} taking into account both the NO and IO types of light neutrino mass spectra consistent with the best fit to the oscillation data. It is clear from Fig. 8 (left-panel) that for this choice of phases given in eq. (55)) in the NO case, even $M_{\Delta_2} = 10^{12}$ GeV fails to generate adequate asymmetry within the experimental range for any value of μ_{Δ_2}. But the left-panel of the same Fig. 8 also shows that the required value of baryon asymmetry can be successfully generated for $M_{\Delta_2} = 2 \times 10^{12}$ GeV and higher values. Right-panel of Fig. 8 shows that for IO case $M_{\Delta_2} = 10^{12}$ GeV is enough to generate baryon asymmetry within the experimental range.

Now we choose a specific set of triplet mass and trilinear coupling ($M_{\Delta_2} = 5 \times 10^{12}$, $\mu_{\Delta_2} = 2.6 \times 10^{11}$ GeV) for NO case, and ($M_{\Delta_2} = 5 \times 10^{12}$, $\mu_{\Delta_2} = 2.1 \times 10^{11}$ GeV) for IO case. We show the evolution of relevant variables of Boltzmann equation as a function of $z(= M_{\Delta_2}/T)$ in Fig. 9 and Fig. 10 for the NO and IO cases, respectively.

4.2. *Flavoured regime*

As already discussed above, the flavoured regime can be approximately subdivided into two: (i) the two-flavoured or τ-flavoured regime for which $10^9 < \frac{M_{\Delta_2}}{\text{GeV}} < 4 \times 10^{11}$, and (ii) the three-flavoured or fully flavoured regime for which $M_{\Delta_2} < 10^9$ GeV. For the sake of simplicity throughout the present work we confine our discussion to the 'two-flavoured or τ-flavoured' regime only. Here we take the mass of the lighter triplet (M_{Δ_2}) to be less than 4×10^{11} but greater than 10^9 GeV. Therefore, according to the discussion presented in Sec. 2.3, the decoherence of τ flavour has been achieved fully whereas e and μ still act as a coherent superposition which can be treated equivalently as a single flavour $a \equiv e + \mu$. Thus here we have two distinguish-

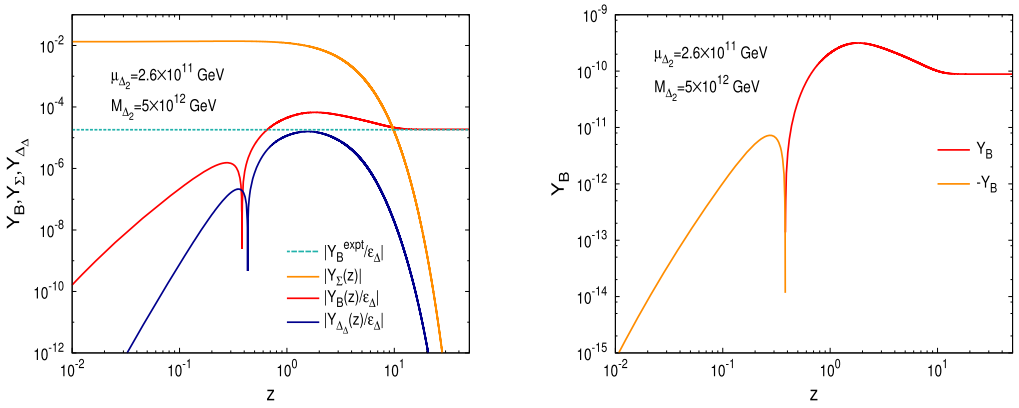

Fig. 9. Left-panel: Evolutions of different variables of the Boltzmann equation with z for the fixed set ($M_{\Delta_2} = 5 \times 10^{12}, \mu_{\Delta_2} = 2.6 \times 10^{11}$ GeV) in NO case. The horizontal dashed line represents the experimental value of baryon asymmetry. Right panel: variation of Y_B with z for the same fixed set of ($M_{\Delta_2}, \mu_{\Delta_2}$) as in the left-panel.

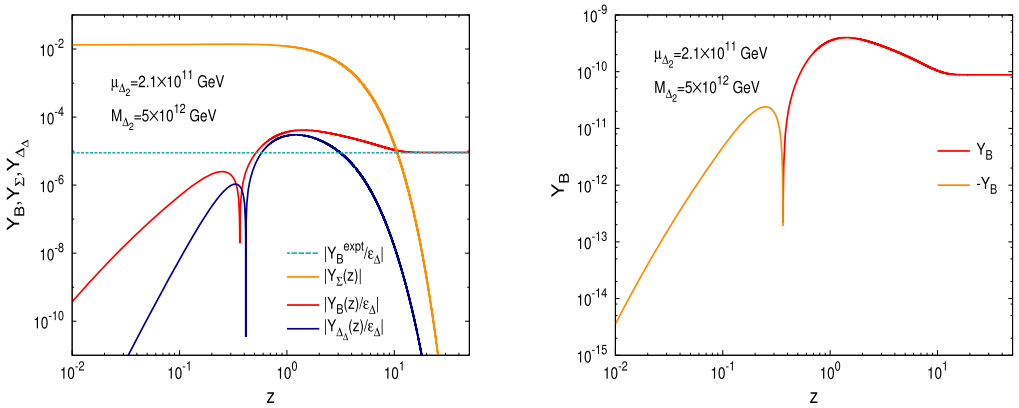

Fig. 10. Left-panel: Evolutions of different variables of the Boltzmann equation with z for the fixed set ($M_{\Delta_2} = 5 \times 10^{12}, \mu_{\Delta_2} = 2.1 \times 10^{11}$ GeV) in IO case. The horizontal dashed line represents the experimental value of baryon asymmetry. Right-panel: Variation of Y_B with z for the same fixed set of ($M_{\Delta_2}, \mu_{\Delta_2}$) as in the left-panel.

able flavours a and τ.[5] Accordingly we have two flavoured CP asymmetry parameters ϵ^{τ}_{Δ} and ϵ^{a}_{Δ} where $\Delta \equiv \Delta_2$ and $\epsilon^{a}_{\Delta} = \epsilon^{e}_{\Delta} + \epsilon^{\mu}_{\Delta}$. They can be calculated using the set of formulas given in eq. (10), eq. (11), and eq. (12) of Sec. 2.1 for flavoured CP asymmetry. Those flavoured CP asymmetry parameters are then used in the set of flavoured Boltzmann equations in eq. (25), eq. (26), and eq. (27) which have to be solved simultaneously upto a very high value of z in order to derive the final freeze-in value of baryon asymmetry Y_B. In the process of these computations we bear in mind that the lepton flavour indices (i, j, k) in those equations can take only two values a and τ. Therefore, the asymmetry vector $\vec{Y}_{\Delta}$ in this case consists of three entries given by $\left[\vec{Y}_{\Delta}\right]^T \equiv \left(Y_{\Delta_\Delta}, Y_{B/3-L_a}, Y_{B/3-L_\tau}\right)$. It can be understood that the dimensionality of the

[5] Hence the nomenclature of this regime as 2-flavoured or τ-flavoured regime is well known [31].

asymmetries coupling matrices C^{l}_{ij}, C^{ϕ}_{k} will be 2×3 and 1×3, respectively and their explicit numerical forms are given in Table 4 of Appendix A.3. The branching ratios ($B_{l_{ij}}$) of triplet decay to different lepton flavours can be regarded as a 2×2 matrix of the form

$$B_l = \begin{pmatrix} B_{l_{aa}} & B_{l_{a\tau}} \\ B_{l_{\tau a}} & B_{l_{\tau\tau}} \end{pmatrix}. \tag{56}$$

The 22 element is obvious $B_{l_{\tau\tau}} = \frac{M_{\Delta_2}}{8\pi\Gamma^{tot}_{\Delta_2}}|y^{(2)}_{33}|^2$, whereas the other three entries are given by

$$B_{l_{aa}} = \frac{M_{\Delta_2}}{8\pi\Gamma^{tot}_{\Delta_2}}\sum_{i,j=1,2}|y^{(2)}_{ij}|^2, \tag{57}$$

$$B_{l_{a\tau}} = \frac{M_{\Delta_2}}{8\pi\Gamma^{tot}_{\Delta_2}}\sum_{i=1,2}|y^{(2)}_{i3}|^2, \tag{58}$$

$$B_{l_{\tau a}} = \frac{M_{\Delta_2}}{8\pi\Gamma^{tot}_{\Delta_2}}\sum_{j=1,2}|y^{(2)}_{3j}|^2\,. \tag{59}$$

We are now in a position to solve the set of flavoured Boltzmann equations to find the value of the asymmetry parameters $Y_{B/3-L_a}(z\to z_f)$, $Y_{B/3-L_\tau}(z\to z_f)$ where z_f is a large enough value of z where asymmetry freezes, i.e. it does not change furthermore with decrease in temperature T. Then the final baryon asymmetry parameter Y_B is evaluated by summing over $Y_{B/3-L_a}(z_f)$, $Y_{B/3-L_\tau}(z_f)$ followed by multiplication with sphaleronic factor and the $SU(2)$ factor as shown in eq. (31). Now the detailed numerical analysis has been subdivided in two categories depending upon the phase differences and modulus ratios in a manner similar to that of the unflavoured case.

4.2.1. Identical ratio and phase differences connecting $m^{(1)}_{\nu}$ and $m^{(2)}_{\nu}$

For numerical computations we use a fixed modulus ratio and phase difference as $F_{ij}=0.1$ and $(\phi^{(1)}_{ij}-\phi^{(2)}_{ij}) = -\pi/2$ for all $i,\,j$. Numerical values of the light neutrino mass matrix elements $(m_\nu)_{ij}$ have been obtained by using the best fit values of the neutrino oscillation data with NO type mass hierarchy of eq. (43). The rest of the analysis has been carried out for two fixed benchmark values of the lighter triplet mass in the range 10^9 GeV $< M_{\Delta_2} < 4\times 10^{11}$ GeV. The trilinear LNV coupling μ_{Δ_2} is taken over a wider range of values while keeping the ratio $\frac{\mu_{\Delta_2}}{M_{\Delta_2}}$ within the perturbative limit. After gathering information about all the required quantities, we first estimate the flavoured CP asymmetry parameters of eq. (10), eq. (11) and eq. (12). In this context, it should be mentioned that the flavour violating (or the purely flavoured) part of the CP asymmetry parameter $\epsilon^{l_i(\not{L})}_{\Delta}$ of eq. (12) vanishes identically since the phase differences $(\phi^{(1)}_{ij}-\phi^{(2)}_{ij})$ are assumed to be identical for any combination of $i,\,j$. Therefore only the combined CP-asymmetry with (lepton number + flavour) violating part $\epsilon^{l_i(\not{L},\not{I})}_{\Delta}$ contributes to the asymmetry generation.

For NO type light neutrino mass hierarchy, the (Y_B) parameter dependence on the trilinear coupling (μ_{Δ_2}) is shown in Fig. 11 for two fixed benchmark values of $M_{\Delta_2} = 10^{11}, 4\times 10^{11}$ GeV. For both the values of the triplet mass, the curve intersects the horizontal line representing experimental baryon asymmetry at two places. It signifies that for each fixed value of the triplet mass, enough asymmetry within the experimental range can be generated with two distinct values

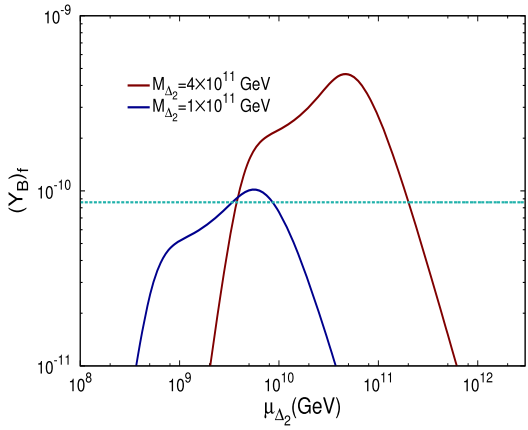

Fig. 11. Variation of baryon asymmetry with trilinear coupling for two fixed benchmark values of the triplet mass ($M_{\Delta_2} = 10^{11}$ GeV and $M_{\Delta_2} = 4 \times 10^{11}$ GeV) in the NO case. The horizontal dashed line represents the experimental value of baryon asymmetry.

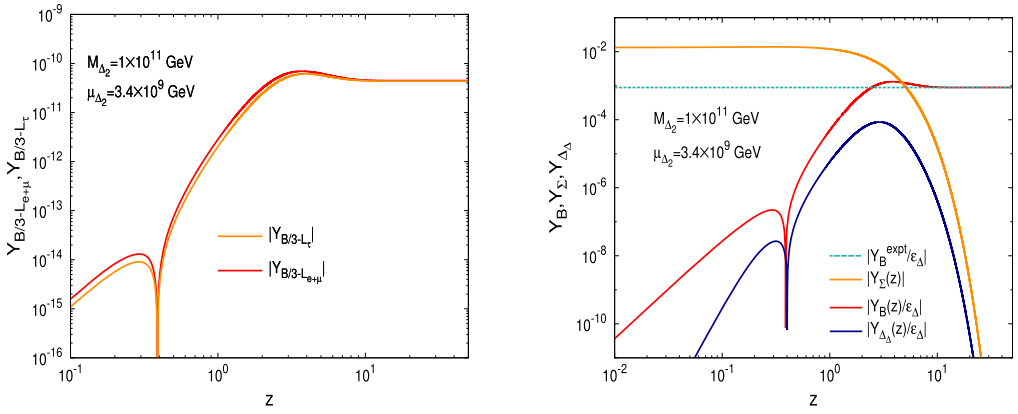

Fig. 12. Left-panel: Evolutions of different flavour asymmetry parameters with z for the fixed set ($M_{\Delta_2} = 10^{11}, \mu_{\Delta_2} = 3.4 \times 10^9$ GeV). Right-panel: Variation of $Y_\Sigma, Y_{\Delta_\Delta}, Y_B$ with z for the same fixed set of $(M_{\Delta_2}, \mu_{\Delta_2})$. The horizontal dashed line represents the experimental value of baryon asymmetry. The whole analysis has been carried out using NO type light neutrino masses and the best fit.

of trilinear coupling μ_{Δ_2}, one before and the other after the peak of the curve. Picking one such combination of triplet mass and trilinear coupling ($M_{\Delta_2} = 10^{11}, \mu_{\Delta_2} = 3.4 \times 10^9$ GeV) we show the evolution of different flavour asymmetry parameters with z in the left-panel of Fig. 12 while the right-panel of the same figure depicts the variations of triplet density abundance (Y_Σ), triplet asymmetry (Y_{Δ_Δ}) and the baryon asymmetry parameter (Y_B)[6] which for a large value of z freezes to the experimental value (shown by dashed line).

[6] In Fig. 12 we have scaled the variables Y_{Δ_Δ}, Y_B by sum of absolute value of the flavoured CP asymmetry parameters ($\varepsilon_\Delta = |\epsilon_\Delta^{e+\mu}| + |\epsilon_\Delta^{\tau}|$) to show all of them ($Y_\Sigma, Y_{\Delta_\Delta}, Y_B$) in same figure.

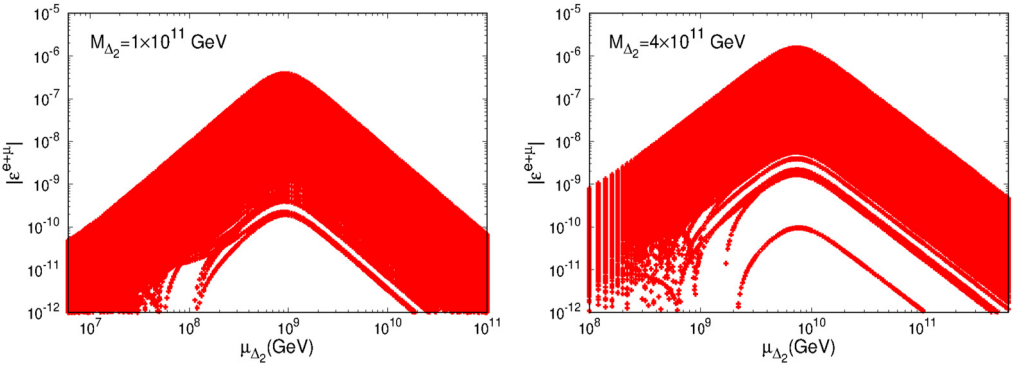

Fig. 13. CP asymmetry parameter corresponding to the flavour $a \equiv e + \mu$ for a wide range of values of μ_{Δ_2}. The thick spread along the vertical axis signifies N number of values of the asymmetry parameter corresponding to N random sets of phase differences. Left-panel: $M_{\Delta_2} = 10^{11}$ GeV (fixed); Right-panel: $M_{\Delta_2} = 4 \times 10^{11}$ GeV (fixed).

4.2.2. Identical ratio but random phase differences connecting $m_\nu^{(1)}$ and $m_\nu^{(2)}$

Following exactly the same procedure as in Sec. 4.1.2 we generate large number of sets of random phase differences $\Phi_{k=1,\ldots N}(N = \text{large integer})$ while taking identical values for all ratios $\mathcal{F}_{k=1,\ldots.N} = \{0.1, 0.1, 0.1, 0.1, 0.1, 0.1\}$. Although theoretically we can find the baryon asymmetry for all these N number of sets, practically it is too time consuming. So we choose one specific set among those N number of sets. Particularly, we select that set which will produce maximum CP asymmetry. For this purpose we choose two fixed values of the lighter triplet mass $M_{\Delta_2} = 10^{11}, 4 \times 10^{11}$ GeV, while permitting μ_{Δ_2} over a wide range. For each combination of $(M_{\Delta_2}, \mu_{\Delta_2})$ the flavoured CP asymmetries are computed taking into account all of the (N) random sets of phases.[7] The resulting plot is shown in Fig. 13 where the spread in values of CP asymmetry for a fixed value of μ_{Δ_2} arises due to the N random sets. Then we pick the top most value of CP asymmetry from the plot and the set of phase differences as $\frac{\Phi_{k=k_{max}}}{\pi} = \{-0.711, -2.228, -1.798, -1.606, -1.809, -1.481\}$. Only this very set is used for all the future numerical computations. One interesting aspect of this scenario is that here we can have non-trivial value of the flavour violating (or purely flavoured) CP asymmetry parameter $(\epsilon_\Delta^{l_i(\not{L})})$ due to the unequal values of phase differences $(\phi_{ij}^{(1)} - \phi_{ij}^{(2)})$ $(i, j = 1, 3)$ for different combinations of i, j. We examine whether the allowed range of parameters can meet the requirement of purely flavoured leptogenesis (PFL) (i.e. $(\epsilon_\Delta^{l_i(\not{L})} \gg \epsilon_\Delta^{l_i(\not{L},\not{L})})$). In Fig. 14 we show the relative magnitudes of the two components (only F violating, $(L + F$ violating)) of the CP asymmetry parameter corresponding to the flavour $a \equiv e + \mu$ for a wide range of μ_{Δ_2} for each value of M_{Δ_2} kept fixed at 10^{11} GeV or 4×10^{11} GeV. It is clear from Fig. 14 that PFL condition is satisfied only over a short range of values of μ_{Δ_2}, i.e. $\mu_{\Delta_2} \lesssim 10^6$ GeV when M_{Δ_2} fixed at 10^{11} GeV and $\mu_{\Delta_2} \lesssim 10^7$ GeV for $M_{\Delta_2} = 4 \times 10^{11}$ GeV. But the resulting values of the total CP asymmetry within these above mentioned range are too small $(\epsilon_\Delta^{e+\mu} \sim 10^{-12} - 10^{-11})$ to produce enough baryon asymmetry. To get higher values of CP asymmetry we have to go to the higher values of μ_{Δ_2} for which $\epsilon_\Delta^{l_i(\not{L},\not{L})}$ increases but $\epsilon_\Delta^{l_i(\not{L})}$ decreases with μ_{Δ_2} and, eventually, the (lepton number+flavour) violating asymmetry becomes much larger than the flavour violating one so

[7] Here we have taken $N = 10000$, i.e. 10000 random sets have been generated.

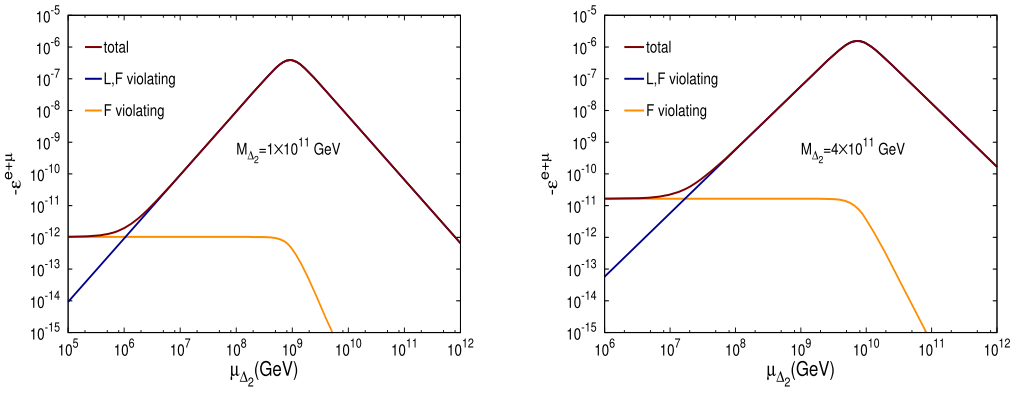

Fig. 14. Relative magnitude of different components of the CP asymmetry parameter corresponding to the flavour $a \equiv e + \mu$ for a wide range of values of μ_{Δ_2}. Left panel: $M_{\Delta_2} = 10^{11}$ GeV (fixed); Right panel: $M_{\Delta_2} = 4 \times 10^{11}$ GeV (fixed).

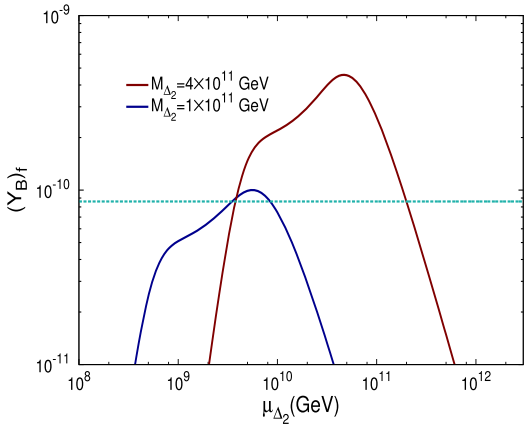

Fig. 15. Variation final value of baryon asymmetry with trilinear coupling for two fixed benchmark values of lighter triplet mass ($M_{\Delta_2} = 10^{11}$ GeV and $M_{\Delta_2} = 4 \times 10^{11}$ GeV). The horizontal dashed line represents the experimental value of baryon asymmetry (the whole analysis has been carried out assuming NO for light neutrino masses).

that the total asymmetry merges with the $(\not{L}, \not{F})$ component, i.e. $\epsilon_\Delta^{l_i} \simeq \epsilon_\Delta^{l_i(\not{L},\not{F})}$. For successful leptogenesis (i.e. to generate baryon asymmetry at the experimental order through leptogenesis), the value of CP asymmetry required is around $(\sim 10^{-8} - 10^{-6})$ depending upon the mass of the lighter triplet. When the total CP-asymmetry lies around the range mentioned above, the flavour violating component $\epsilon_\Delta^{l_i(\not{F})}$ is negligibly small and total asymmetry can be considered to be constituted solely by the (lepton number+flavour) violating part ($\epsilon_\Delta^{l_i(\not{L},\not{F})}$) which is clear from Fig. 14. Therefore the discussions following Fig. 14 allow us to conclude that although we can generate adequate baryon asymmetry (Y_B) through flavoured leptogenesis, condition of PFL can not be satisfied. In other words in the regime where PFL condition is satisfied, the resulting CP asymmetry comes out to be so small that it can not generate Y_B within the experimental range.

We now plot the final values of the baryon asymmetry parameter $(Y_B)_f$ as a function of the trilinear coupling (μ_{Δ_2}) in Fig. 15 for two fixed benchmark values of the triplet mass (M_{Δ_2}). Both

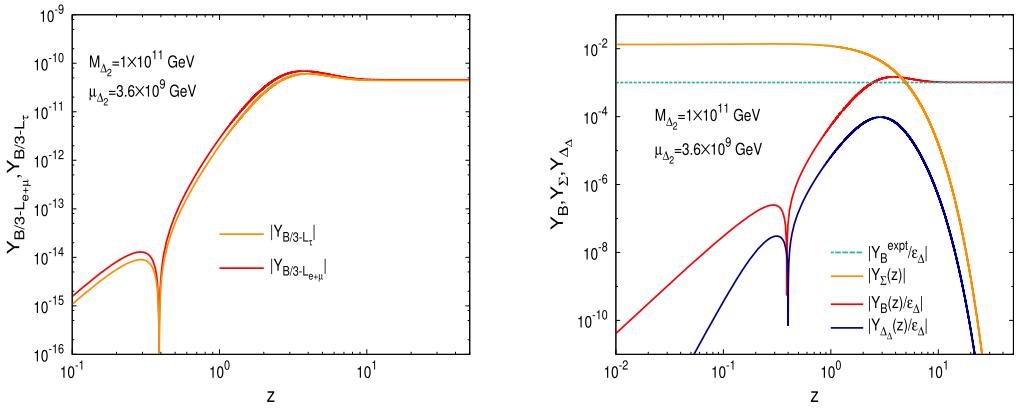

Fig. 16. Left-panel: Evolution of baryon asymmetry parameters with z for fixed values of $(M_{\Delta_2} = 10^{11}, \mu_{\Delta_2} = 3.6 \times 10^9$ GeV) using best fit to neutrino oscillation data with NO type light neutrino masses. Right panel: Variation of $Y_\Sigma, Y_{\Delta_\Delta}, Y_B$ with z for the same fixed set of $(M_{\Delta_2}, \mu_{\Delta_2})$. The horizontal dashed line represents the experimental value of baryon asymmetry.

the curves $((Y_B)_f$ vs $(\mu_{\Delta_2}))$ intersect the horizontal dashed line representing the experimental value of Y_B at two places which in turn indicates that for each fixed value of (M_{Δ_2}) there are two $(M_{\Delta_2}, \mu_{\Delta_2})$ combinations which successfully generates the desired value of baryon asymmetry in the experimental range. Out of the two intersecting points located on the horizontal line in the $(Y_B)_f$ vs (μ_{Δ_2}) curve, we choose the extreme left point corresponding to fixed $M_{\Delta_2} = 10^{11}$ GeV curve which identifies this point with $(M_{\Delta_2} = 10^{11}, \mu_{\Delta_2} = 3.6 \times 10^9$ GeV)). Correspondingly we show the variation of flavour asymmetry parameters $(Y_{B/3-L_{e+\mu}}, Y_{B/3-L_\tau})$ with z in the left panel of Fig. 16 while the right panel of the same figure depicts the evolution of other variables occurring in solutions of Boltzmann equations including the baryon asymmetry. The left-panel and the right-panel of this figure clearly indicate that, for this specific choice of parameters, the baryon asymmetry finally freezes-in to the desired constant value within the experimental range at a large enough value of z (or at sufficiently low temperature).

5. Minimal model extension for dark matter and vacuum stability

The inert scalar doublet model has radiative seesaw ansatz for neutrino masses and intrinsic capability for dark matter [50] which has been also shown to originate from SO(10) [51] with matter parity [52–54] as the stabilising discrete symmetry. More recently new possible origin of scotogenic dark matter stability has been also suggested from softly broken global lepton number symmetry $U(1)_L$ [55]. This inert doublet model [50] also does not have vacuum instability problem in the associated scalar potential. But the two heavy Higgs scalar triplet model [15] (or the purely triplet seesaw model [31]), as such, does not possess dark matter through which it can explain cosmological evidences including the observed relic density $(\Omega_{\rm DM}h^2 = 0.1172 - 0.1224)$ [5,6,43]. The expected DM mass has been also bounded from direct and indirect detection experiments [39–42]. This issue has been also addressed in a number of ways in SM extensions through a singlet scalar representing a weakly interacting massive particle (WIMP) [46] as DM candidate and the investigations have been also updated more recently in [47]. But most of the models discussed in [47] and earlier have not addressed neutrino oscillation data, cosmological bound, and baryon asymmetry via leptogenesis. Also they have not addressed the issue on the

Table 2
Singlet scalar extensions of the two Higgs triplet model [15] and its particle content with respective charges under $G_{213} \times Z_2$ symmetry. The second and the third generation fermions not shown in this Table have identical transformation properties.

Particle	SM charges	Z_2 charge
$(\nu, e)_L^T$	$(2, -1/2, 1)$	-1
e_R	$(1, -1, 1)$	-1
$(u, d)_L^T$	$(2, 1/6, 3)$	-1
u_R	$(1, 2/3, 3)$	-1
d_R	$(1, -1/3, 3)$	-1
ϕ	$(2, 1/2, 1)$	$+1$
Δ_1	$(3, -1, 1)$	$+1$
Δ_2	$(3, -1, 1)$	$+1$
ξ	$(1, 0, 1)$	-1

vacuum stability of the associated scalar potential [44,45]. Using corresponding renormalisation group evolutions (RGEs) discussed in the Appendix we find that in the two heavy Higgs triplet model [15] with $M_{\Delta_i}(i = 1, 2) \geq 10^{13}$ GeV, although the stability has been improved by predicting the Higgs quartic coupling λ_ϕ to be positive in an extended region with $|\phi| \geq 10^{13}$ GeV, the problem has not been completely resolved. In particular, we note that in this model [15] the standard Higgs quartic coupling λ_ϕ runs negative in the interval $|\phi| \simeq 10^{10} - 10^{13}$ GeV showing the persistence of vacuum instability of the scalar potential [44,45]. Such instability also persists in the more recent investigation of the two-triplet model [31]. In this section we discuss how the heavy Higgs triplet model that accounts for neutrino mass and baryon asymmetry as discussed above can also be easily extended further to account for the phenomena of WIMP DM while completing vacuum stability through the same scalar DM. We add a real scalar singlet ξ to the two Higgs triplet model [15] and assume an additional Z_2 discrete symmetry under which ξ and all SM fermions are odd. All other scalars including the SM Higgs ϕ and the two triplets are assumed to possess $Z_2 = +1$. Thus the resulting Lagrangian after this real scalar extension has the symmetry $SU(2)_L \times U(1)_Y \times SU(3)_C \times Z_2 (\equiv G_{213} \times Z_2)$. The particle content and their charges in the minimally extended model under this symmetry are shown in Table 2.

5.1. Real scalar singlet dark matter

At all lower mass scales $\mu \ll M_{\Delta_i}(i = 1, 2)$ noting that the two heavy Higgs triplets in the Lagrangian of [15] are expected to have decoupled leading, effectively, to the SM scalar potential $\mu \ll M_{\Delta_i}(i = 1, 2)$**:**

$$V_{SM} = -\mu_H^2 \phi^\dagger \phi + \lambda_\phi (\phi^\dagger \phi)^2. \tag{60}$$

It is well known that this SM potential alone develops vacuum instability as the quartic coupling λ_ϕ runs negative at energy scales $\mu \geq 5 \times 10^9$ GeV [44,45]. In models with type-I see saw extensions of the SM, the negativity of λ_ϕ is further enhanced due to RHN Yukawa interactions. This latter type of enhancement due to RHN is absent in the purely triplet leptogenesis model [15]. Using renormalisation group equations discussed in the Appendix we find that the SM Higgs quartic coupling remains positive for field values $|\phi| \leq 5 \times 10^9$ GeV and $|\phi| \geq 10^{13}$ GeV where the latter limit is due to $M_{\Delta_2} = 10^{13}$ GeV in [15]. Although such positive values of Higgs quartic coupling is a considerable improvement over purely SM running, the model [15] does

not resolve the vacuum instability issue completely. This is due to the fact that standard Higgs quartic coupling in the model [15] acquires negative values in the region $|\phi| \simeq 5 \times 10^9$ GeV to $|\phi| \simeq 10^{13}$ GeV. Further details of discussion of this problem has been made below in Sec. 5.1.3.

In order to resolve both the issues on DM and vacuum stability of the scalar potential, we make a simple extension of the model [15] by adding a real scalar singlet ξ whose mass we determine from DM relic density, direct detection experimental bounds and vacuum stability fits. For the stability of DM we impose a Z_2 discrete symmetry under which ξ and all SM fermions are odd, but all other scalars in the extended model are even under Z_2 as shown in Table 2. The scalar potential is now modified in the presence of ξ for mass scales $\mu < M_{\Delta_2}$

$$V_\xi = V_{SM} + \mu_\xi^2 \xi^2 + \lambda_\xi \xi^4 + 2\lambda_{\phi\xi}(\phi^\dagger\phi)\xi^2. \tag{61}$$

In eq. (61) λ_ξ = dark matter self coupling, $\lambda_{\phi\xi}$ = Higgs portal coupling and μ_ξ = mass of ξ. The VEV of the standard Higgs doublet redefines the DM mass parameter

$$\begin{aligned} M_{DM}^2 &= 2(\mu_\xi^2 + \lambda_{\phi\xi}^2 v^2), \\ m_\phi^2 &= 2\mu_H^2 = 2\lambda_\phi v^2. \end{aligned} \tag{62}$$

For mass scales $\mu \geq M_{\Delta_2}$ the Higgs potential receives additional contributions due to $\Delta_i (i = 1, 2)$ and its interactions with others

$\mu \geq M_{\Delta_2}$:

$$\begin{aligned} V_{\xi\Delta} = V_\xi &+ \sum_{(i=1,2)} \left(M_{\Delta_i}^2 \mathrm{Tr}(\Delta_i^\dagger \Delta_i) + \lambda_1^i [\mathrm{Tr}(\Delta_i^\dagger \Delta_i)]^2 + \lambda_2^i [\mathrm{Tr}(\Delta_i^\dagger \Delta_i)]^2 - \mathrm{Tr}[(\Delta_i^\dagger \Delta_i)^2] \right) \\ &+ \sum_{(i=1,2)} \left(\lambda_3^i (\phi^\dagger\phi)\mathrm{Tr}(\Delta_i^\dagger \Delta_i) + \lambda_4^i \phi^\dagger [(\Delta_i^\dagger \Delta_i) - (\Delta_i \Delta_i^\dagger)]\phi \right. \\ &\left. + \left[\frac{\mu_i}{\sqrt{2}} \phi^T i\tau_2 \Delta_i^\dagger \phi + H.c. \right] \right) \\ &+ \sum_{(i=1,2)} \lambda_\xi^i \mathrm{Tr}(\Delta_i^\dagger \Delta_i)\xi^2 \end{aligned} \tag{63}$$

where V_ξ has been defined in eq. (61).

In order to examine the allowed values of the Higgs portal coupling $\lambda_{\phi\xi}$, we use two different kinds of experimental results: (i) bounds on cosmological DM relic density [5,43] $\Omega_{\mathrm{DM}}h^2 = 0.1172 - 0.1224$, (ii) bounds from DM direct detection experiments such as LUX-2016 [39], XENON1T [40,41] and PANDA-X-II [42]. Using our ansatz we estimate the relic densities for different combinations of $m_\xi, \lambda_{\phi\chi}$. It is then easy to restrict the values of m_ξ and $\lambda_{\phi\xi}$ using the bound on relic density mentioned above. In direct detection experiments it is assumed that WIMPs passing through earth scatter elastically from the target material of the detector. The energy transfer to the detector nuclei can be measured through various types of signals. All those direct detection experiments provide DM mass vs DM-nucleon scattering cross section plot which clearly separates the allowed regions below the predicted curve from the forbidden regions above the curve.

5.1.1. Estimation of dark matter relic density

We assume the WIMP DM particle ξ to have decoupled from the thermal bath at some early epoch which has thus remained as a thermal relic. The following conventions are used at a certain stage of evolution of the Universe. Denoting $\Gamma =$ particle decay rate and $H =$ Hubble parameter, a particle species is said to be coupled if $\Gamma > H$. Similarly it is assumed to have decoupled if $\Gamma < H$. The corresponding Boltzmann equation [56,57] is solved for the estimation of the particle relic density

$$\frac{dn}{dt} + 3Hn = -\langle \sigma v_0 \rangle (n^2 - n_{eq}^2) \tag{64}$$

Here $n =$ actual number density of ξ at a certain instant of time, $n_{eq} =$ its equilibrium number density, $v_0 =$ velocity of ξ, and $\langle \sigma v_0 \rangle =$ thermally averaged DM annihilation cross section. Approximate solution of Boltzmann equation gives the expression for the relic density [57,58]

$$\Omega_{\rm DM} h^2 = \frac{1.07 \times 10^9 x_F}{\sqrt{g_*} M_{pl} \langle \sigma v_0 \rangle} \tag{65}$$

where $x_F = m_\xi / T_F$, $T_F =$ freeze-out temperature, $g_* =$ effective number of massless degrees of freedom and $M_{pl} = 1.22 \times 10^{19}$ GeV. This x_F can be computed by iteratively solving the equation

$$x_F = \ln \left(\frac{m_\xi}{2\pi^3} \sqrt{\frac{45 M_{pl}^2}{8 g_* x_F}} \langle \sigma v_0 \rangle \right). \tag{66}$$

In eq. (65) and eq. (66), the only particle physics input is the thermally averaged annihilation cross section. The total annihilation cross section is obtained by summing over all the annihilation channels of the singlet DM which are $\xi\xi \to F\bar{F}, W^+W^-, ZZ, hh$ where the symbol F represents all the associated fermions of SM. Using the expression of total annihilation cross section [59–61] in eq. (66) at first we compute x_F which is then utilised in eq. (65) to yield the relic density. Two free parameters involved in this computation are mass of the DM particle m_ξ and the Higgs portal coupling $\lambda_{\phi\xi}$. The relic density has been estimated for a wide range of values of the DM matter mass ranging from few GeVs to few TeVs while the coupling $\lambda_{\phi\xi}$ is also varied simultaneously in the range $(10^{-4} - 1)$. The parameter space $(m_\xi, \lambda_{\phi\xi})$ is thus constrained by using the bound on the relic density reported by WMAP [43] and Planck [5]. In Fig. 17 we show only those combinations of $\lambda_{\phi\xi}$ and m_ξ which are capable of producing relic density in the experimentally observed range.

5.1.2. Dark matter mass bounds from direct detection experiments

We get exclusion plots of DM-nucleon scattering cross section and DM mass from different direct detection experiments. The spin independent scattering cross section of singlet DM on nucleon is [62]

$$\sigma^{\rm SI} = \frac{f_n^2 \lambda_{\phi\xi}^2 \mu_R^2 m_N^2}{4\pi m_\xi^2 m_h^4} \ ({\rm cm}^2), \tag{67}$$

where $m_h =$ mass of the SM Higgs ($\sim$ 125 GeV), $m_N =$ nucleon mass $\sim$ 939 MeV, $\mu_R = (m_\xi m_N)/(m_\xi + m_N) =$ reduced DM-nucleon mass and the factor $f_n \sim 0.3$. Using eq. (67) the exclusion plots in the $\sigma - m_\xi$ plane can be easily brought to $\lambda_{\phi\xi} - m_\xi$ plane. We superimpose

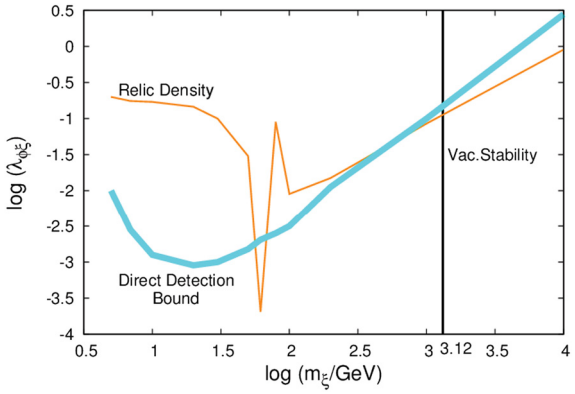

Fig. 17. Determination of dark matter mass from observed relic density, direct detection experiments, and vacuum stability: The yellow curve denotes the values of the parameters $(\lambda_{\phi\xi}, m_\xi)$ allowed by the relic density bound ($\Omega_{\rm DM}h^2 = 0.1172 - 0.1224$). The cyan band represents overlapping exclusion plots from direct detection experiments of LUX-2016, XENON1T(2017) and PANDA-XII(2017) for which any region below (above) the green band is allowed (forbidden). The vertical line at $\log(m_\xi) = 3.1$ ($m_\xi = 1.3$ TeV) is due to limit set by vacuum stability of the scalar potential as discussed in Sec. 5.1.3. (For interpretation of the colours in the figure(s), the reader is referred to the web version of this article.)

the $\lambda_{\phi\xi}$ versus m_ξ plots for different experiments on the plot of allowed parameter space constrained by relic density bound resulting in Fig. 17. Thus the Fig. 17 exhibits the parameter space $(\lambda_{\phi\xi}\ vs.\ m_\xi)$ constrained by both the relic density bound and the direct detection experiments.

From Fig. 17 we note that the points on the yellow curve lying below the green band are allowed by both relic density and direct detection experiments. This predicts lower values of DM mass in the region $m_\xi \simeq 59 - 63$ GeV for the Higgs portal coupling $\lambda_{\phi,\xi} \leq 10^{-3}$ which is too small to be compatible with vacuum stability completion discussed below in Sec. 5.1.3. All other values of DM masses $m_\xi \geq 750$ GeV are also allowed by relic density and direct detection experimental constraints. But as discussed below this region will be further constrained by vacuum stability criteria.

5.1.3. Resolution of vacuum instability

We have examined vacuum stability of different scalar potentials encountered in different regions of Higgs field value $\mu = |\phi|$ starting from $\mu = m_{top} - M_{Planck}$ through the renormalisation group evolutions (RGEs) of the standard Higgs (ϕ) quartic coupling in the respective cases [63–66] which have been given in Sec. A.4 of the Appendix. At first using RGEs for Higgs quartic coupling λ_ϕ and gauge and top quark Yukawa couplings for the SM alone in the absence of DM ξ or heavy triplets, we have plotted the quartic coupling against standard Higgs field values $\mu = |\phi| = m_{top} - M_{Planck}$. As already noted [44,45] $\lambda_\phi(\mu)$ runs negative for all field values $\mu \geq 5 \times 10^9$ GeV clearly exhibiting vacuum instability of the SM Higgs potential. This has been shown by the lower curve in Fig. 18. We next examined the evolution of $\lambda_\phi(\mu)$ in the two-heavy Higgs triplet extension model [15] using $M_{\Delta_2} \simeq M_{\Delta_1} \simeq 10^{13}$ GeV but in the absence of DM ξ. Besides being positive for $\mu < 5 \times 10^9$ GeV, the Higgs potential became definitely positive for field values $\mu \geq 10^{13}$ GeV with considerable improvement on the stability. However, the quartic coupling is found to be negative for field values in the range $\mu = 5 \times 10^9$ GeV to $\mu = 10^{13}$ GeV as demarcated by the two vertical green dashed lines in Fig. 18). We next included the effect of DM ξ and the Higgs portal coupling $\lambda_{\phi\xi}$ through the DM modified Higgs potential V_ξ ignor-

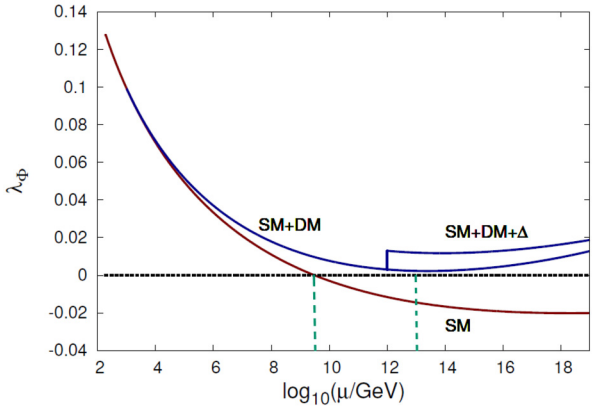

Fig. 18. Renormalization group evolution of Higgs quartic coupling (denoted as λ_Φ) as a function of scalar field value $\mu = |\phi|$ showing presence of vacuum instability in the SM (lower red curve) for $\mu > 5 \times 10^9$ GeV. The vertical green dashed lines represent boundaries of the region within which λ_ϕ runs negative for 5×10^9 GeV $< \mu < M_{\Delta_2} \simeq 10^{13}$ GeV in the model of [15]. The middle blue curve marked as SM+DM represents evolution of λ_ϕ in the presence of real scalar DM ξ, excluding triplets, in the present model extension. Additional RG correction in the present model due to triplet masses has been shown by the uppermost curve marked as SM+DM+Δ where threshold enhancement due to Δ_2 mass has been also included.

ing the presence of Higgs triplets in the model extension. The quartic coupling λ_ϕ was found to be positive in the entire region of Higgs field values until the Planck mass. This behaviour has been shown by the upper curve in Fig. 18 excluding the threshold like enhancement at $\mu = 10^{12}$ GeV. Finally the combined effects of DM ξ and the heavy Higgs triplets have been included on the Higgs quartic coupling running where the effect of heavy Higgs triplets occurs only for $\mu \geq M_{\Delta_2}$. In this region we have taken $\lambda_1^{(2)} = \lambda_2^{(1)} \simeq 0.15$ and ignored the effect of all other quartic couplings by setting their starting values to be negligibly small. We have also retained small threshold effect due to Δ_2 resulting in $\Delta\lambda_\phi = \frac{\mu_{\Delta_2}^2}{M_{\Delta_2}^2}$. Due to allowed heavier mass of Δ_1 its threshold effect has been treated to be negligible.

Initial values of the Higgs quartic coupling λ_ϕ, DM self coupling λ_ξ, DM Higgs portal coupling $\lambda_{\phi\xi}$, SM gauge couplings g_Y, g_{2L}, g_{3c}, and the top quark Yukawa coupling h_t used for RG evolution have been shown in Table 3 for $m_\xi = 1.3$ TeV and $m_\xi = 2$ GeV. We find that at $m_\xi = 1.3$ TeV, the one-loop evolution of λ_ϕ reaches its minimum positive value around $|\phi| = 10^{13}$ GeV. But if $m_\xi < 1.3$ TeV, then λ_ϕ tends to run negative in the region $10^{11} - 10^{12}$ GeV even in the presence of heavy triplets which have their masses $> 10^{11}$ GeV in the present investigation. This leads us to conclude that the vacuum stability predicts the real scalar DM mass to be $m_\xi \geq 1.3$ TeV. As the direct detection cross section rapidly decreases with increasing m_ξ in this region, the predicted mass $m_\xi = 1.3$ TeV is expected to be more accessible to experiments compared to values $m_\xi \gg 1.3$ TeV, although the latter values are also allowed by the three constraints:relic density, direct detection, and vacuum stability.

5.1.4. Summary of dark matter mass prediction

We summarize below the results of theoretical and computational analyses on DM mass carried out in this section

Table 3
Initial values of coupling constants at top quark mass $\mu = m_{top} = 173.34$ GeV [67,68] for different values of the scalar singlet dark matter mass m_ξ. The input values of gauge couplings $g_i\,(i = Y, 2L, 3C)$ and top-quark Yukawa coupling h_t are due to PDG data [69] as explained in the Appendix. The predicted values of $\lambda_{\phi\xi}$ and m_ξ are obtained from the plot of constrained parameter space of Fig. 17. Values mentioned in 4th to 8th columns are common to all the dark matter masses.

m_χ (TeV)	$\lambda_{\phi\xi}$	λ_ξ	λ_ϕ	g_{1Y}	g_{2L}	g_{3C}	h_t
0.75	0.075	0.190					
1.3	0.118	0.220					
1.5	0.140	0.165	0.129	0.35	0.64	1.16	0.94
2	0.158	0.100					

- Although the DM mass values in the narrow region $m_\xi = 59 - 63$ GeV are permitted by both relic density [43,70] and direct detection measurements, the corresponding Higgs portal coupling values $\lambda_{\phi,\xi} \simeq 1.7 \times 10^{-4} - 1.6 \times 10^{-3}$ are too small to complete vacuum stability of the scalar potential.
- All DM mass values $m_\xi \geq 750$ GeV easily satisfy both the relic density and the direct detection constraints. But for masses 0.75 TeV $< m_\xi <$ 1.3 TeV, the corresponding input values of $\lambda_{\phi,\xi}$ yield negative values for the RG evolution of λ_ϕ in the region $|\phi| \simeq 10^{10} - 10^{11}$ GeV leading to vacuum instability of the scalar potential.
- Thus, we find that the present minimal extension of the two-triplet model predicts real scalar singlet DM mass $m_\xi \geq 1300$ GeV that satisfies all the three constraints: relic density, direct detection, and vacuum stability of the scalar potential. Out of these, the lowest limit $m_\xi =$ 1.3 TeV is expected to be comparatively more sensitive and accessible to direct detection experiments.

6. Radiative stability of Higgs mass and naturalness

In the present two-triplet model there are couplings of SM Higgs scalar (ϕ) with triplets which are likely to introduce large radiative correction $\delta m_\phi \propto M_{\Delta_1} \simeq 10^{13}$ GeV, the highest mass scale in the theory. This would destabilise the SM Higgs mass prediction and electroweak gauge hierarchy, and calls for exploring naturalness criteria [37,38,71,72], if any, to restrict such correction not to exceed the observed Higgs mass. A number of investigations have been carried out to constrain certain non-SUSY seesaw model parameters to stabilise the Higgs mass near the electroweak scale [37,38,71,72]. In this section we discuss how a naturalness constraint is available within this two-triplet model without upsetting the model predictions for neutrino mass, leptogenesis, dark matter, and vacuum stability discussed in previous sections.

The Feynman diagrams with loop-mediation by the components of the two heavy Higgs triplets are shown in Fig. 19. Neglecting the contribution of the second diagram in Fig. 19 which is $\propto v^2$, those due to the other two diagrams add up to

$$\delta m_\phi^2 = \frac{-3}{16\pi^2}\left([\lambda_3^{(1)} + \frac{1}{2}|\lambda_6^{(1)}|^2]M_{\Delta_1}^2[1 + \ln(\frac{\Lambda_R^2}{M_{\Delta_1}^2})]\right) + \frac{-3}{16\pi^2}\left([\lambda_3^{(2)} + \frac{1}{2}|\lambda_6^{(2)}|^2]M_{\Delta_2}^2[1 + \ln(\frac{\Lambda_R^2}{M_{\Delta_2}^2})]\right). \quad (68)$$

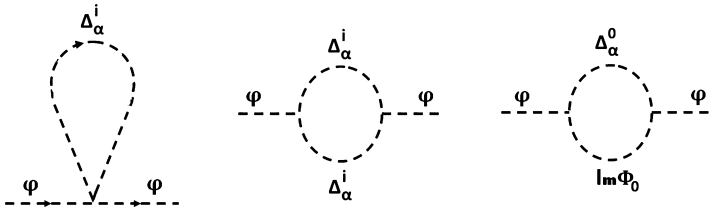

Fig. 19. Feynman diagrams showing one-loop corrections to the standard Higgs mass mediated by charged and neutral components of two heavy scalar triplets $\Delta^i_\alpha(\alpha = 1, 2; i = \pm\pm, \pm)$. Here $Im\Phi_0$ is the imaginary part of the neutral component of standard Higgs doublet Φ.

As explained earlier, the dimensionless couplings $\lambda_6^{(j)} = \frac{\mu_j}{M_{\Delta_j}}(j = 1, 2)$ are known from fitting the oscillation data and our leptogenesis ansatz in various cases leading to wider range of values for $\lambda_6^{(2)}$. The first (second) line in eq. (68) represents the dominant radiative corrections to the Higgs mass due to the heavy triplet $\Delta_1(\Delta_2)$. Using the regularisation scale $\Lambda_R = M_{\Delta_1}$ which is the highest scalar mass in this model gives

$$\delta m_\phi^2 = (\frac{-3}{16\pi^2})\left([\lambda_3^{(1)} + \frac{1}{2}|\lambda_6^{(1)}|^2]M_{\Delta_1}^2 + [\lambda_3^{(2)} + \frac{1}{2}|\lambda_6^{(2)}|^2]M_{\Delta_2}^2 R_L\right), \tag{69}$$

where

$$R_L = 1 + \ln(\frac{M_{\Delta_1}^2}{M_{\Delta_2}^2}). \tag{70}$$

Eq. (69) leads to

$$\frac{\delta m_\phi^2}{m_\phi^2} = 0.019\left[\frac{M_{\Delta_1}}{100\ \text{GeV}}\right]^2\left(\lambda_3^{(1)} + \frac{1}{2}|\lambda_6^{(1)}|^2 + [\lambda_3^{(2)} + \frac{1}{2}|\lambda_6^{(2)}|^2]R_\Delta R_L\right), \tag{71}$$

where

$$R_\Delta = \frac{M_{\Delta_2}^2}{M_{\Delta_1}^2}. \tag{72}$$

The naturalness criteria then suggest that RHS of eq. (71) ≤ 1. Thus the present model can be consistent with naturalness if the quantity inside the parenthesis in the RHS of this eq. (71) is fine tuned to be zero and such cancellation should be ensured at least upto $2n_\delta - 4$ places after the decimal point where $\frac{M_{\Delta_1}}{GeV} = 10^{n_\delta}$. For this purpose we note that although $0.1 \leq R_\Delta < 1$ and $R_L > 1$, the product $0.1 < R_\Delta R_L < 1$ which make the cancellation possible within the perturbative limits of $\lambda_3^{(i)}(i = 1, 2)$. Contrary to various constraints available on $\phi\phi\Delta\Delta$ quartic couplings [73] in one-triplet extensions of the SM [72], there does not seem to exist similar bounds in two-Higgs triplet model except for the universal perturbativity bound.

With fixed values of $(M_{\Delta_1} = 3 \times 10^{13}, \mu_{\Delta_1} = 10^{13})$ GeV but for three different sets of $(M_{\Delta_2} = 5 \times 10^{12}, \mu_{\Delta_2} = 2 \times 10^{11})$ GeV, $(2 \times 10^{12}, \mu_{\Delta_2} = 7.7 \times 10^{10})$ GeV, and $(10^{12}, \mu_{\Delta_2} = 1.1 \times 10^{11})$ GeV, allowed by neutrino mass and unflavoured leptogenesis, we make a parametric representation of the naturalness criteria for those values of $(\lambda_3^{(1)}\text{vs.}\lambda_3^{(2)})$ for which the RHS of eq. (71) vanishes. These three domains of naturalness solutions are presented by respective straight lines designated by the corresponding values of parameters as shown in Fig. 20.

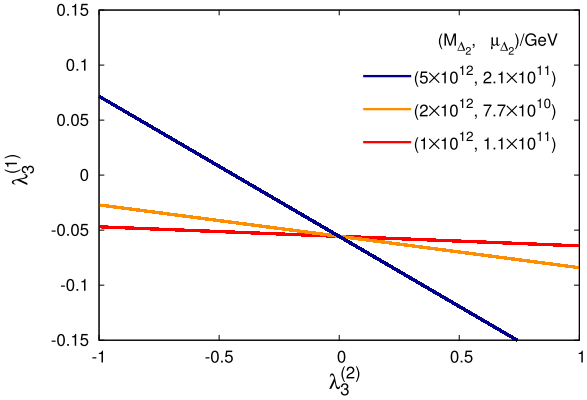

Fig. 20. Allowed domains for fine-tuned naturalness solution in the two-heavy triplet seesaw and leptogenesis model consistent with neutrino mass, baryon asymmetry of the Universe, vacuum stability, and one-loop radiative stability of Higgs mass.

From Fig. 20 we find that the naturalness constraint that keeps RHS of eq. (71) ≤ 1 is satisfied for all quartic couplings well within the perturbative limits. Some of the numerical values of $\lambda_3^{(i)}(i = 1, 2)$ satisfying naturalness constraint as shown in Fig. 20 have been already taken into account in the RGE of $\lambda_\phi(\mu)$ in our vacuum stability ansatz of Sec. 5.1.3. Contributions of other larger values of these quartic couplings $\lambda_3^{(i)}(i = 1, 2)$ are found to keep the values of $\lambda_\phi(\mu)$ well below the perturbative limit even at $\mu \simeq M_{Planck}$. We have checked that similar plots displaying naturalness constraints on the quartic couplings are possible for other two-flavoured leptogenesis solutions with $M_{\Delta_2} = 1 \times 10^{11}$ GeV and $M_{\Delta_2} = 4 \times 10^{11}$ GeV. Particularly, the small $\lambda_3^{(i)}(i = 1, 2)$ solutions represented by red and orange coloured straight lines in Fig. 20 might be relevant for quantum gravity [74] which predicts all quartic couplings to vanish for $\mu > M_{Planck}$.

We thus conclude that the two triplet model can confront the Higgs mass naturalness problem via fine tuning of the model parameters without affecting neutrino mass, leptogenesis, dark matter and vacuum stability predictions.

7. Summary and outlook

The original suggestion of purely triplet seesaw and leptogenesis [15] addresses the interesting new possibility that both neutrino masses and baryon asymmetry of the universe can be explained using only two heavy Higgs triplets in the absence of right-handed neutrinos. If neutrinos are quasi-degenerate with relatively larger mass scale, they can predict baryon asymmetry of the universe [15] while manifesting in experimentally verifiable double beta decay. Noting that the recently determined cosmological bounds due to Planck satellite data has severely restricted the sum of three neutrino masses to < 0.23 eV (or even smaller bound < 0.12 eV), and the recent neutrino oscillation data have revealed θ_{23} to be in the second octant with large Dirac CP-phase ($\simeq 214°$), in this work we have examined this model predictions with hierarchical neutrino masses satisfying these cosmological bounds in concordance with the neutrino oscillation data.

We have also attempted to explore the model potential in addressing current issues on dark matter and vacuum stability of the scalar potential through a simple minimal extension of the

model [15]. We find that the original model can explain both the recent neutrino oscillation data while successfully predicting baryon asymmetry of the universe for both normal and inverted orderings where our best fit is consistent with the sum of the three neutrino masses to be nearly 25%(50%) of the Planck satellite bound reported in [5] ([28]).

We have further shown the possibilities of both unflavoured and two-flavoured leptogenesis leading to experimental values of baryon asymmetry through detailed solutions to the respective set of CP-asymmetries and Boltzmann equations where the numerical results are consistent with generic choice of the two constituent light neutrino mass matrices $(m_\nu^{(1)}, m_\nu^{(2)})$. It has been shown (through proper graphical illustration) that adequate asymmetry as quoted by the experiments can be successfully generated even if elements of those two matrices are connected by completely random phases.

In addition we have also found that a simple minimal extension of the two-Higgs triplet model [15] successfully predicts a real scalar single dark matter in agreement with observed relic density and mass bounds set by direct and indirect detection experiments. Noting that in the scalar potential of the original model [15], the standard Higgs quartic coupling λ_ϕ runs negative in the region 5×10^9 GeV $\leq |\phi| \leq 10^{13}$ GeV, we have shown how the presence of this real scalar singlet DM also completes the vacuum stability. The lowest limit of the DM mass $m_\xi \simeq 750$ GeV that satisfies the existing data and constraints due to relic density and direct and indirect detection experiments, is further pushed to 1.3 TeV under the constraint of vacuum stability completion.

Noting that the two-triplet model, as such, is likely to destabilise the electroweak gauge hierarchy through large Higgs mass radiative correction, we have also found the corresponding naturalness constraint on the model parameters that restricts this correction not to exceed the observed value of the Higgs mass itself. This naturalness constraint on model parameters does not affect our successful predictions of neutrino mass, leptogenesis, baryon asymmetry, dark matter and vacuum stability.

In conclusion we note that the purely triplet seesaw model for neutrino mass and leptogenesis [15] is capable of successfully describing the most recent neutrino oscillation data including θ_{23} in the second octant and large Dirac CP-phase for both normal and inverted ordering of neutrino masses in concordance with the existing cosmological bounds determined from Planck satellite measurement. Being non-supersymmetric the model has no gravitino problem and has a natural advantage of predicting cosmologically safe relic abundance of light elements. Supplemented by the underlying naturalness criteria the model is capable of ensuring Higgs mass radiative stability. We further conclude that a simple minimal extension of this model [15] successfully explains the direct and indirect evidences of dark matter; it also completes vacuum stability of the scalar potential. Thus, a simple and minimal extension of the original model [15] is capable of solving current puzzles confronting the SM: neutrino oscillation and baryon asymmetry of the universe within the cosmological bound but without gravitino problem, dark matter, vacuum stability, and Higgs mass radiative stability.

Although the dark matter stabilising Z_2 discrete symmetry has been assumed in the present model extension based upon the symmetry $SU(2)_L \times U(1)_Y \times SU(3)_C \times Z_2$ in the spirit of numerous other models including [21,47,50,75,76], it would be interesting to explore its deeper gauge theoretic origin as in [51–53,77,78] from unified model perspectives [33,54,79]. Because

of dark-matter portal couplings with triplets, $\lambda_\xi^{(i)} (i = 1, 2)$, the real scalar DM mass prediction may be unstable against one loop radiative correction. But the model has a DM mass stability constraint similar to eq. (71) that can restrict the radiative correction close to or less than m_ξ through fine-tuning of these couplings.

Declaration of competing interest

The authors declare that they have no known competing financial interests or personal relationships that could have appeared to influence the work reported in this paper.

Acknowledgement

M. K. P. acknowledges financial support through the research project **SB/S2/HEP-011/2013** awarded by the Department of Science and Technology, Government of India. M.C. would like to acknowledge the financial support provided by SERB-DST, Govt. of India through the project **EMR/2017/001434**. S.K.N. and R.S. acknowledge the award of their Ph. D. research scholarships by Siksha 'O' Anusandhan, Deemed to be University.

Appendix A

A.1. Number density of particle species

The number densities for the massive as well as massless particles (assuming Maxwell Boltzmann distribution for both) are given by [31,32]

$$n_\Sigma^{eq}(z) = n_\Delta^{eq}(z) + n_N^{eq}(z)^\dagger \,, \tag{73}$$

$$n_\Delta^{eq}(z) = \frac{3M_\Delta^3 K_2(z)}{2\pi^2 z}, \tag{74}$$

$$n_{l,\phi}^{eq}(z) = \frac{2M_\Delta^3}{\pi^2 z}, \tag{75}$$

where $K_2(z)$ is the modified Bessel function of second kind. The expressions of entropy density and Hubble parameter are listed below.

$$s(z) = \frac{4g^* M_\Delta^3}{\pi^2 z^3}, \tag{76}$$

$$H(z) = \sqrt{\frac{8g^*}{\pi^2}} \frac{M_\Delta}{M_{\rm Planck} z^2}, \tag{77}$$

with effective relativistic degrees of freedom $g^* = 106.75$ and Planck mass $M_{\rm Planck} = 1.22 \times 10^{19}$ GeV.

A.2. Reaction densities

Decay $(1 \to 2)$ related reaction densities for lightest scalar triplet is given by [31,32]

$$\gamma_D = \frac{K_1(z)}{K_2(z)} n_\Sigma^{eq}(z) \Gamma_\Delta^{tot} \tag{78}$$

where Γ_{Δ}^{tot} is the total triplet decay width. The generic expression of $(2 \leftrightarrow 2)$ scattering reaction densities is given by

$$\gamma_s = \frac{M_{\Delta}^4}{64\pi^4} \int_{x_{min}}^{\infty} \sqrt{x} \frac{(z\sqrt{x})\hat{\sigma_s}}{z} dx \tag{79}$$

where $x = s'/M_{\Delta}^2$ (s' is the centre of mass energy) and $\hat{\sigma_s}$ denotes reduced cross section. For gauge induced process $x_{min} = 4$ and Yukawa induced process it is $x_{min} = 0$. The reduced cross sections for the gauge induced processes are given by [31,32]

$$\begin{aligned}\hat{\sigma_A} = \frac{2}{72\pi} \Big\{ & (15C_1 - 3C_2)\omega + (5C_2 - 11C_1)\omega^3 + 3(\omega^2 - 1)[2C_1 + C_2(\omega^2 - 1)] \\ & \times \ln\Big(\frac{1+\omega}{1-\omega}\Big)\Big\} \\ & + \Big(\frac{50 g_{2L}^4 + 41 {g_{1Y}}^4}{48\pi}\Big)\omega^{\frac{3}{2}},\end{aligned} \tag{80}$$

where $\omega \equiv \omega(x) = \sqrt{1 - 4/x}$ and $C_1 = 12g_{2L}^4 + 3g_{1Y}^4 + 12g_{2L}^2 g_{1Y}^2$, $C_2 = 6g_{2L}^4 + 3g_{1Y}^4 + 12g_{2L}^2 g_{1Y}^2$. ($g_{2L}$ is the SM $SU(2)$ coupling and g_{1Y} is the SM $U(1)_Y$ coupling.) Reduced cross sections of $\Delta L = 2$ scattering processes (s channel and t channel respectively) are given by

$$\hat{\sigma}_{l_i l_j}^{\phi\phi} = 64\pi\, B_{\phi} B_{l_{ij}} \delta^2 \Big[\frac{x}{(x-1)^2 + \delta^2}\Big], \tag{81}$$

$$\hat{\sigma}_{\phi l_j}^{\phi l_j} = 64\pi\, B_{\phi} B_{l_{ij}} \delta^2 \frac{1}{x}\Big[\ln(1+x) - \frac{x}{1+x}\Big], \tag{82}$$

where $\delta = \Gamma_{\Delta}^{tot}/M_{\Delta}$. Similarly the reduced cross sections for lepton flavor violating processes (s channel and t channel) are represented as

$$\hat{\sigma}_{l_i l_j}^{l_n l_m} = 64\pi\, B_{l_{nm}} B_{l_{ij}} \delta^2 \Big[\frac{x}{(x-1)^2 + \delta^2}\Big], \tag{83}$$

$$\hat{\sigma}_{l_i l_n}^{l_j l_m} = 64\pi\, B_{l_{nm}} B_{l_{ij}} \delta^2 \Big[\frac{x+2}{x+1} - \ln(1+x)\Big]. \tag{84}$$

Reaction densities of different scattering processes ($\gamma_A, \gamma_{l_i l_j}^{\phi\phi}, \gamma_{l_i l_j}^{l_n l_m}$ etc) can be calculated using the expressions of reduced cross sections (eq. (80)–eq. (84)) in the generic formula (eq. (79)) for the scattering reaction density. The Resonant intermediate state subtracted reaction densities are given by

$$\gamma'^{\phi\phi}_{l_i l_j} = \gamma_{l_i l_j}^{\phi\phi} - B_{l_{ij}} B_{\phi} \gamma_D \tag{85}$$

$$\gamma'^{l_n l_m}_{l_i l_j} = \gamma_{l_i l_j}^{l_n l_m} - B_{l_{ij}} B_{l_{nm}} \gamma_D\ . \tag{86}$$

A.3. C^l and C^{ϕ} matrices

The lepton asymmetry and scalar doublet asymmetry are related to $(B/3 - L_i)$ and triplet asymmetry through the asymmetry coupling matrices C^l and C^{ϕ}. These matrices are determined by solving a constrained set (imposed by Global symmetry of the Lagrangian and chemical equilibrium relations) of equations involving chemical potentials. Above a certain temperature ($\sim 10^{12}$ GeV) the lepton flavours act as a single entity (a coherent superposition of three flavours

Table 4
C^l and C^ϕ matrices in different temperature regimes.

T (GeV)	Flavours	C^l	C^ϕ
$\gtrsim 10^{15}$	single	$\begin{pmatrix} 0 & \frac{1}{2} \end{pmatrix}$	$\begin{pmatrix} 3 & \frac{1}{2} \end{pmatrix}$
$[10^{12}, 10^{15}]$		$\begin{pmatrix} 0 & \frac{1}{2} \end{pmatrix}$	$\begin{pmatrix} 2 & \frac{1}{3} \end{pmatrix}$
$[T^\tau_{decoh}, 10^{12}]$		$\begin{pmatrix} 0 & \frac{3}{10} \end{pmatrix}$	$\begin{pmatrix} \frac{3}{4} & \frac{1}{8} \end{pmatrix}$
$[10^9, T^\tau_{decoh}]$, $[T^\mu_{decoh}, T^\tau_{decoh}]$	two	$\begin{pmatrix} -\frac{6}{359} & \frac{307}{718} & -\frac{18}{359} \\ \frac{39}{359} & -\frac{21}{718} & \frac{117}{359} \end{pmatrix}$	$\begin{pmatrix} \frac{258}{359} & \frac{41}{359} & \frac{56}{359} \end{pmatrix}$
$[10^5, T^\mu_{decoh}]$	three	$\begin{pmatrix} -\frac{6}{179} & \frac{151}{358} & -\frac{10}{179} & -\frac{10}{179} \\ \frac{33}{358} & -\frac{25}{716} & \frac{172}{537} & -\frac{7}{537} \\ \frac{33}{358} & -\frac{25}{716} & -\frac{7}{537} & \frac{172}{537} \end{pmatrix}$	$\begin{pmatrix} \frac{123}{179} & \frac{37}{358} & \frac{26}{179} & \frac{26}{179} \end{pmatrix}$
$\lesssim 10^5$		$\begin{pmatrix} -\frac{9}{158} & \frac{221}{711} & -\frac{16}{711} & -\frac{16}{711} \\ \frac{9}{158} & -\frac{16}{711} & \frac{221}{711} & -\frac{16}{711} \\ \frac{9}{158} & -\frac{16}{711} & -\frac{16}{711} & \frac{221}{711} \end{pmatrix}$	$\begin{pmatrix} \frac{39}{79} & \frac{8}{79} & \frac{8}{79} & \frac{8}{79} \end{pmatrix}$

(e, μ, τ)). The lepton flavour decoherence temperature (which signifies the temperature at which a specific lepton flavour loses its coherence and can be treated as a separate entity) is denoted by $T^{f_i}_{decoh}$, where f_i stands for any specific flavour (e, μ, τ). So it is clear that above a temperature T^τ_{decoh} all three lepton flavours act indistinguishably and the Boltzmann equation has to be solved for the quantity $(B - L)$. Again the regime $T > T^\tau_{decoh}$ is subdivided into three windows. The structure of C^l and C^ϕ matrices are different in those windows since the number of active chemical potentials and the governing constraint equations are different in each of these windows (This issue has been discussed extensively in Sec. 3.1 and Appendix B of Ref. [31]). Similarly in the intermediate region between $T^\tau_{decoh} - T^\mu_{decoh}$ two lepton flavours $(a(\equiv e + \mu), \tau)$ are effectively active, whereas below T^μ_{decoh} complete flavour decoherence is attained and all three lepton flavours are separately identifiable, thus the set of flavoured Boltzmann equations has to be solved in terms of $(B/3 - L_e, B/3 - L_\mu, B/3 - L_\tau)$. The asymmetry coupling matrices (following Ref. [31]) are shown in Table 4.

A.4. Renormalisation group equations for gauge and scalar couplings

We use the following electroweak precision data at $\mu \simeq m_{top}$ and the Higgs mass [67–69] as inputs in the bottom-up approach

$$\begin{aligned} m_{top} &= 173.34 \pm 0.77 \text{ GeV} \\ \sin^2\theta_W &= 0.23129 \pm 0.00005 \\ \alpha_S &= 0.1182 \pm 0.0005 \\ \frac{1}{\alpha} &= 127.9 \pm 0.02 \\ m_h &= 125.09 \pm 0.237 \text{ GeV} \end{aligned} \tag{87}$$

These values determine the initial boundary values $\lambda_\phi = 0.129$, the SM gauge couplings $g_{1Y} = 0.35$, $g_{2L} = 0.64$, $g_{3C} = 1.16$ and the top-quark Yukawa coupling $h_t = 0.94$. In addition we use the Higgs triplet masses, their trilinear couplings, and scalar singlet DM mass as discussed in Sec. 3, Sec. 4, Sec. 5 and Sec. 5.1,

$$\begin{aligned} M_{\Delta_2} &= 10^{12}\ \text{GeV} \\ \mu_{\Delta_2} &= 6\times 10^{10}\ \text{GeV} \\ m_\xi &= 1.3\ \text{TeV} \\ M_{\Delta_1} &= 10^{13}\ \text{GeV} \\ \mu_{\Delta_1} &= 10^{12}\ \text{GeV}. \end{aligned} \tag{88}$$

The RGEs for SM gauge couplings and top quark Yukawa coupling at two loop level are given by

$$\begin{aligned} \frac{dh_t}{d\ln\mu} &= \frac{1}{16\pi^2}\left(\frac{9}{2}h_t^2 - \frac{17}{12}g_{1Y}^2 - \frac{9}{4}g_{2L}^2 - 8g_{3C}^2\right)h_t \\ &+ \frac{1}{(16\pi^2)^2}[-\frac{23}{4}g_{2L}^4 - \frac{3}{4}g_{2L}^2 g_{1Y}^2 + \frac{1187}{216}g_{1Y}^4 + 9g_{2L}^2 g_{3C}^2 + \frac{19}{9}g_{3C}^2 g_{1Y}^2 - 108g_{3C}^4 \\ &+ \left(\frac{225}{16}g_{2L}^2 + \frac{131}{16}g_{1Y}^2 + 36g_{3C}^2\right)h_t^2 + 6(-2h_t^4 - 2h_t^2\lambda_\phi + \lambda_\phi^2)], \\ \frac{dg_{1Y}}{d\ln\mu} &= \frac{1}{16\pi^2}\left(\frac{41}{6}g_{1Y}^3\right) + \frac{1}{(16\pi^2)^2}\left(\frac{199}{18}g_{1Y}^2 + \frac{9}{2}g_{2L}^2 + \frac{44}{3}g_{3C}^2 - \frac{17}{6}h_t^2\right)g_{1Y}^3, \\ \frac{dg_{2L}}{d\ln\mu} &= \frac{1}{16\pi^2}\left(-\frac{19}{6}g_{2L}^3\right) + \frac{1}{(16\pi^2)^2}\left(\frac{3}{2}g_{1Y}^2 + \frac{35}{6}g_{2L}^2 + 12g_{3C}^2 - \frac{3}{2}h_t^2\right)g_{2L}^3, \\ \frac{dg_{3C}}{d\ln\mu} &= \frac{1}{16\pi^2}\left(-7g_{3C}^3\right) + \frac{1}{(16\pi^2)^2}\left(\frac{11}{6}g_{1Y}^2 + \frac{9}{2}g_{2L}^2 - 26g_{3C}^2 - 2h_t^2\right)g_{3C}^3, \end{aligned} \tag{89}$$

where g_{2L}, g_{1Y}, g_{3C} are the gauge couplings of $SU(2)_L, U(1)_Y, SU(3)_C$, respectively, and h_t is the top quark Yukawa coupling. The RG equations for the scalar quartic couplings up to one loop level are

$$\begin{aligned} \frac{d\lambda_\phi}{d\ln\mu} &= \frac{1}{16\pi^2}\Bigg[(12h_t^2 - 3{g_{1Y}}^2 - 9g_{2L}^2)\lambda_\phi - 6h_t^4 + \frac{3}{8}\{2g_{2L}^4 + ({g_{1Y}}^2 + g_{2L}^2)^2\} \\ &\quad + 24\lambda_\phi^2 + 4\lambda_{\phi\xi}^2\Bigg], \\ \frac{d\lambda_{\phi\xi}}{d\ln\mu} &= \frac{1}{16\pi^2}\left[\frac{1}{2}(12h_t^2 - 3{g_{1Y}}^2 - 9g_{2L}^2)\lambda_{\phi\xi} + 4\lambda_{\phi\xi}(3\lambda_\phi + 2\lambda_\xi) + 8\lambda_{\phi\xi}^2\right], \\ \frac{d\lambda_\xi}{d\ln\mu} &= \frac{1}{16\pi^2}\left[8\lambda_{\phi\xi}^2 + 20\lambda_\xi^2\right]. \end{aligned} \tag{90}$$

For mass scale $\mu \geq M_{\Delta_2} \simeq 10^{12}$ GeV, the scalar potential is defined through eq. (63) of Sec. 5.1.

We define the respective beta functions through

$$16\pi^2\frac{dC}{dt} = \beta_C \quad (C = \lambda_\phi, \lambda_{\phi\xi}, \lambda_\xi, \lambda_1^i, \lambda_2^i, \lambda_3^i, \lambda_4^i, (i = 1, 2)). \tag{91}$$

The beta functions for desired quartic couplings are

$$\beta_{\lambda_\phi} = \lambda_\phi \left[12\lambda_\phi - \left(\frac{9}{5} g_{1Y}^2 + 9 g_{2L}^2 \right) + 12 h_t^2 \right] + \frac{9}{4} \left(\frac{3}{25} g_{1Y}^4 + \frac{2}{5} g_{1Y}^2 g_{2L}^2 + g_{2L}^4 \right) + \sum_{(i=1,2)} \left(6(\lambda_3^i)^2 + 4(\lambda_4^i)^2 \right) - 12 h_t^4, \tag{92}$$

For $i = 1, 2$, the RGEs for respective quartic couplings are

$$\beta_{\lambda_1^i} = \lambda_1^i \left[14\lambda_1^i + 4\lambda_2^i - \left(\frac{36}{5} g_{1Y}^2 + 24 g_{2L}^2 \right) + 4\mathrm{Tr}[T] \right] + \frac{108}{25} g_{1Y}^4 + \frac{72}{5} g_{1Y}^2 g_{2L}^2 + 18 g_{2L}^4 + 2(\lambda_2^i)^2 + 4(\lambda_3^i)^2 + 4(\lambda_4^i)^2 - 8\mathrm{Tr}\left[T^2\right], \tag{93}$$

$$\beta_{\lambda_2^i} = \lambda_2^i \left[12\lambda_1^i + 3\lambda_2^i - \left(\frac{36}{5} g_{1Y}^2 + 24 g_{2L}^2 \right) + 4\mathrm{Tr}[T] \right] - \frac{144}{5} g_{1Y}^2 g_{2L}^2 + 12 g_{2L}^4 - 8(\lambda_4^i)^2 + 8\mathrm{Tr}\left[T^2\right], \tag{94}$$

$$\beta_{\lambda_3^i} = \lambda_3^i \left[6\lambda_\phi + 8\lambda_1^i + 2\lambda_2^i + 4\lambda_3^i - \left(\frac{9}{2} g_{1Y}^2 + \frac{33}{2} g_{2L}^2 \right) + 6 h_t^2 + 2\mathrm{Tr}[T] \right] + \frac{27}{25} g_{1Y}^4 + 6 g_{2L}^4 + 8(\lambda_3^i)^2 - 4\mathrm{Tr}\left[T^2\right], \tag{95}$$

$$\beta_{\lambda_4^i} = \lambda_4^i \left[2\lambda^i + 2\lambda_1^i - 2\lambda_2^i + 8\lambda_3^i - \left(\frac{9}{2} g_{1Y}^2 + \frac{33}{2} g_{2L}^2 \right) + 6 h_t^2 + 2\mathrm{Tr}[T] \right] - \frac{18}{5} g_{1Y}^2 g_{2L}^2 + 4\mathrm{Tr}\left[T^2\right], \tag{96}$$

where T is defined as $T = {y^{(2)}}^\dagger y^{(2)}$ where $y^{(2)} \simeq m_\nu / VL2$ and its beta function is expressed through the relation

$$\beta_T = T \left[6\,T - 3 \left(\frac{3}{5} g_{1Y}^2 + 3 g_{2L}^2 \right) + 2\mathrm{Tr}[T] \right]. \tag{97}$$

We have examined how vacuum stability of the scalar potential in this minimally extended model is ensured by the presence of the scalar singlet DM even with its lowest mass $m_\xi \simeq$ 1.3 TeV and its associated Higgs portal coupling. We have estimated RG evolution of standard Higgs quartic coupling λ_ϕ in the presence of the DM as well as the heavy scalar triplets in the appropriate ranges of mass scales and Higgs field values. When the DM and the triplets are excluded we get the lowermost red curve [44,45] of Fig. 18 of Sec. 5.1.3 where λ_ϕ runs negative for all values of Higgs field $|\phi| > 5 \times 10^9$ GeV showing unstable SM vacuum. When we exclude the scalar DM but include the two heavy triplets as in the original model of [15], the negativity of the quartic coupling persists only in the interval $|\phi| = 5 \times 10^9 - 10^{13}$ GeV after which the quartic coupling has the ability to be positive due to the additional contribution of the triplets. Here a major compensation is caused by the Δ_2-threshold enhancement at $M_{\Delta_2} = 10^{13}$ GeV not shown in Fig. 18. In Fig. 18 the negative part of the red coloured curve bounded by vertical green dashed lines is also predicted by the original model [15] signifying vacuum instability in the model. Excluding the triplets but including DM, the solution is given by the upper blue curve of Fig. 18 marked as SM+DM (excluding threshold enhancement). When effects of heavy triplets are also included along with DM in the present model extension, the RG evolution for the quartic

coupling develops threshold enhancement at $M_{\Delta_2} = 10^{12}$ GeV (rather than 10^{13} GeV of [15]) which has been predicted by matching the baryon asymmetry data in the present analysis. This threshold enhancement is $\Delta\lambda_\phi \simeq \mu^2_{\Delta_2}/M^2_{\Delta_2} \simeq 0.005 - 0.01$. In addition we have also included the effects of small triplet portal couplings using $\lambda_3^{(2)} \simeq \lambda_4^{(2)} \simeq 0.1$. The resulting corrections have been shown by the uppermost curve for $\mu > 10^{12}$ Gev in Fig. 18 of Sec. 5.1.3. This part of the curve has been marked as SM+DM+Δ.

References

[1] G.L. Fogli, E. Lisi, A. Marrone, D. Montanino, A. Palazzo, A.M. Rotunno, Phys. Rev. D 86 (2012) 013012, arXiv:1205.5254 [hep-ph];
T. Schwetz, M. Tortola, J.W.F. Valle, New J. Phys. 13 (2011) 063004, arXiv:1103.0734 [hep-ph].

[2] D.V. Forero, M. Tortola, J.W.F. Valle, Phys. Rev. D 90 (9) (2014) 093006, arXiv:1405.7540 [hep-ph];
M.C. Gonzalez-Garcia, M. Maltoni, T. Schwetz, Nucl. Phys. B 908 (2016) 199–217, arXiv:1512.06856 [hep-ph].

[3] I. Esteban, M.C. Gonzalez-Garcia, A. Hernandez-Cabezudo, M. Maltoni, T. Schwetz, J. High Energy Phys. 01 (2019) 106, arXiv:1811.05487 [hep-ph].

[4] D.N. Spergel, et al., WMAP, Astrophys. J. Suppl. 148 (2003) 175–194, arXiv:astro-ph/0302209 [astro-ph];
E. Komatsu, et al., WMAP, Astrophys. J. Suppl. 180 (2009) 330–376, arXiv:0803.0547 [astro-ph];
G. Hinshaw, et al., WMAP, Astrophys. J. Suppl. 180 (2009) 225–245, arXiv:0803.0732 [astro-ph];
E. Komatsu, et al., WMAP, Astrophys. J. Suppl. 192 (2011) 18, arXiv:1001.4538 [astro-ph.CO].

[5] P.A.R. Ade, et al., Planck, Astron. Astrophys. 571 (2014) A16, arXiv:1303.5076 [astro-ph.CO];
P.A.R. Ade, et al., Planck, Astron. Astrophys. 594 (2016) A13, arXiv:1502.01589 [astro-ph.CO].

[6] F. Zwicky, Helv. Phys. Acta 6 (1933) 110;
D.N. Spergel, et al., WMAP Collaboration, Astrophys. J. Suppl. 170 (2007) 377;
J. Einasto, arXiv:0901.0632 [astro-ph,CO];
G.R. Blumenthal, S.M. Faber, J.R. Primack, M.J. Rees, Nature 311 (1984) 517–525;
J. Angle, et al., XENON10 Collaboration, Phys. Rev. Lett. 107 (2011) 051301;
J. Angle, et al., XENON10 Collaboration, Phys. Rev. Lett. 110 (2013) 249901, arXiv:1104.3088 [astro-ph,CO];
L.E. Strigari, Phys. Rep. 531 (2013) 1–88, arXiv:1211.7090 [astro-ph.CO].

[7] V.A. Kuzmin, V.A. Rubakov, M.E. Shaposhnikov, Phys. Lett. B 191 (1987) 171–173.

[8] P. Minkowski, Phys. Lett. B 67 (1977) 421–428;
M. Gell-Mann, P. Ramond, R. Slansky, in: P. van Nieuwenhuizen, D. Freedman (Eds.), Supergravity, North-Holland, 1979, p. 315;
S.L. Glashow, in: M. Lévy, et al. (Eds.), Quarks and Leptons, Cargèse, Plenum, New-York, 1980, p. 707;
T. Yanagida, in: O. Sawada, A. Sugamoto (Eds.), Proceedings of the Workshop on the Unified Theory and the Baryon Number in the Universe Tsukuba, 1979, p. 95, KEK Report No. 79-18;
R.N. Mohapatra, G. Senjanovic, Phys. Rev. Lett. 44 (1980) 912.

[9] J. Schechter, J.W.F. Valle, Phys. Rev. D 22 (1980) 2227.

[10] M. Fukugita, T. Yanagida, Phys. Lett. B 174 (1986) 45–47.

[11] S. Davidson, E. Nardi, Y. Nir, Phys. Rep. 466 (2008) 105–177, arXiv:0802.2962 [hep-ph].

[12] G. Lazarides, Q. Shafi, C. Wetterich, Nucl. Phys. B 181 (1981) 287;
M.A. Luty, Phys. Rev. D 45 (1992) 455;
A. Acker, H. Kikuchi, E. Ma, U. Sarkar, Phys. Rev. D 48 (1993) 5006, arXiv:hep-ph/9305290;
P.J. O'Donnell, U. Sarkar, Phys. Rev. D 49 (1994) 2118, arXiv:hep-ph/9307279;
M. Flanz, E.A. Paschos, U. Sarkar, Phys. Lett. B 345 (1995) 248, Erratum: Phys. Lett. B 382 (1996) 447, arXiv:hep-ph/9411366;
M. Flanz, E.A. Paschos, U. Sarkar, J. Weiss, Phys. Lett. B 389 (1996) 693, arXiv:hep-ph/9607310;
E. Ma, U. Sarkar, Phys. Rev. D 85 (2012) 075015, arXiv:1111.5350 [hep-ph];
E. Ma, Nucl. Phys. B, Proc. Suppl. 168 (2007) 347–349;
T. Hambye, E. Ma, U. Sarkar, Nucl. Phys. B 590 (2000) 429, arXiv:hep-ph/0006173;
T. Hambye, E. Ma, U. Sarkar, Phys. Rev. D 62 (2000) 015010, arXiv:hep-ph/9911422;
E. Ma, U. Sarkar, Phys. Lett. B 458 (1999) 73–78, arXiv:hep-ph/9812276;
T. Hambye, E. Ma, U. Sarkar, Nucl. Phys. B 590 (2000) 429–452, arXiv:hep-ph/0006173;
T. Hambye, E. Ma, M. Raidal, U. Sarkar, Phys. Lett. B 512 (2001) 373–378, arXiv:hep-ph/0011197;

A. Pilaftsis, Phys. Rev. D 56 (1997) 5431, arXiv:hep-ph/9707235;
A. Pilaftsis, Nucl. Phys. B 504 (1997) 61, arXiv:hep-ph/9702393;
W. Buchmuller, M. Plumacher, Phys. Lett. B 389 (1996) 73, arXiv:hep-ph/9608308;
W. Buchmuller, M. Plumacher, Phys. Lett. B 431 (1998) 354, arXiv:hep-ph/9710460;
W. Buchmuller, P. Di Bari, M. Plumacher, Phys. Lett. B 547 (2002) 128, arXiv:hep-ph/0209301;
W. Buchmuller, P. Di Bari, M. Plumacher, Nucl. Phys. B 643 (2002) 367, Erratum: Nucl. Phys. B 793 (2008) 362, arXiv:hep-ph/0205349;
R. Barbieri, P. Creminelli, A. Strummia, N. Tetradis, Nucl. Phys. B 575 (2000) 61, arXiv:hep-ph/9911315;
K. Hamaguchi, H. Murayama, T. Yanagida, Phys. Rev. D 65 (2002) 043512, arXiv:hep-ph/0109030;
T. Hambye, Nucl. Phys. B 633 (2002) 171, arXiv:hep-ph/0111089;
J.R. Ellis, M. Raidal, Nucl. Phys. B 643 (2002) 229, arXiv:hep-ph/0206174;
G.C. Branco, R. Gonzalez Felipe, F.R. Joaquim, I. Masina, M.N. Rebelo, C.A. Savoy, Phys. Rev. D 67 (2003) 073025, arXiv:hep-ph/0211001;
A. Abada, S. Davidson, A. Ibarra, F.-X. Josse-Michaux, M. Losada, A. Riotto, J. High Energy Phys. 0609 (2006) 010, arXiv:hep-ph/0605281;
L. Covi, E. Roulet, F. Vissani, Phys. Lett. B 384 (1996) 169, arXiv:hep-ph/9605319;
Franco Buccella, Domenico Falcone, Chee Seng Fong, Enrico Nardi, Giulia Ricciardi, Phys. Rev. D 86 (2012) 035012, arXiv:1203.0829 [hep-ph];
S.Y. Khlebnikov, M.E. Shaposhnikov, Nucl. Phys. B 308 (1988) 885;
J.A. Harvey, M.S. Turner, Phys. Rev. D 42 (1990) 3344;
F. Iocco, G. Mangano, G. Miele, O. Pisanti, P.D. Serpico, arXiv:0809.0631 [astro-ph];
Enrico Bertuzzo, Pasquale Di Bari, Luca Marzola, Nucl. Phys. B 849 (2011) 521, arXiv:1007.1641 [hep-ph];
Chee Seng Fong, Enrico Nardi, Antonio Riotto, Adv. High Energy Phys. 2012 (2012) 158303, arXiv:1301.3062 [hep-ph];
W. Buchmuller, P. Di Bari, M. Plumacher, Ann. Phys. 315 (2005) 305, arXiv:hep-ph/0401240;
J.C. Pati, Phys. Rev. D 68 (2003) 072002, arXiv:hep-ph/0209160;
J.C. Pati, Int. J. Mod. Phys. A 18 (2003) 4135–4156;
H. An, Shao-Long Chen, R.N. Mohapatra, Y. Zhang, J. High Energy Phys. 1003 (2010) 124, arXiv:0911.4463;
Pei-Hong Gu, Rabindra N. Mohapatra, Phys. Rev. D 97 (7) (2018) 075014, arXiv:1712.00420;
C. Hagedorn, R.N. Mohapatra, E. Molinaro, C.C. Nishi, S.T. Petcov, Int. J. Mod. Phys. A 33 (05) (2018) 184206;
S.K. Majee, M.K. Parida, A. Raychaudhuri, Phys. Lett. B 668 (2008) 299, arXiv:hep-ph/0807395;
S.K. Majee, M.K. Parida, A. Raychaudhuri, U. Sarkar, Phys. Rev. D 75 (2007) 075003, arXiv:hep-ph/0701179;
M.K. Parida, A. Raychaudhuri, Phys. Rev. D 82 (2010) 093017, arXiv:1007.5082 [hep-ph];
I.K. Cooper, S.F. King, C. Luhn, Nucl. Phys. B 859 (2012) 159–176, arXiv:1110.5676 [hep-ph];
F. Bjorkeroth, F.J. de Anda, Ivo de Mederios Varzielas, S.F. King, J. High Energy Phys. 10 (2015) 104, arXiv:1505.05504 [hep-ph];
P. Chen, G.-J. Ding, S.F. King, J. High Energy Phys. 03 (2016) 206, arXiv:1602.03873;
M. Chianese, B. Fu, S.F. King, J. Cosmol. Astropart. Phys. 03 (2020) 030, arXiv:1910.12916 [hep-ph].

[13] A.S. Joshipura, E.A. Paschos, W. Rodejohann, Nucl. Phys. B 611 (2001) 227–238, arXiv:hep-ph/0104228;
A.S. Joshipura, E.A. Paschos, W. Rodejohann, J. High Energy Phys. 08 (2001) 029, arXiv:hep-ph/0105175 [hep-ph];
W. Rodejohann, Phys. Rev. D 70 (2004) 073010, arXiv:hep-ph/0403236;
E.K. Akhmedov, W. Rodejohann, J. High Energy Phys. 06 (2008) 106, arXiv:0803.2417 [hep-ph];
Thomas Rink, Werner Rodejohann, Kai Schmitz, arXiv:2006.03021 [hep-ph].

[14] B. Adhikary, M. Chakraborty, A. Ghosal, Phys. Rev. D 93 (11) (2016) 113001, arXiv:1407.6173 [hep-ph];
R. Samanta, M. Chakraborty, P. Roy, A. Ghosal, J. Cosmol. Astropart. Phys. 03 (2017) 025, arXiv:1610.10081 [hep-ph];
R. Samanta, M. Chakraborty, J. Cosmol. Astropart. Phys. 1902 (2019) 003, arXiv:1802.04751 [hep-ph];
M. Chakraborty, R. Krishnan, A. Ghosal, J. High Energy Phys. 09 (2020) 025, arXiv:2003.00506 [hep-ph].

[15] E. Ma, U. Sarkar, Phys. Rev. Lett. 80 (1998) 5716, arXiv:hep-ph/9802445.

[16] M. Magg, C. Wetterich, Phys. Lett. B 94 (1980) 61;
T.P. Cheng, L.F. Li, Phys. Rev. D 22 (1980) 2860;
G. Lazarides, Q. Shafi, C. Wetterich, Nucl. Phys. B 181 (1981) 287;
R.N. Mohapatra, G. Senjanovic, Phys. Rev. D 23 (1981) 165;
J. Schecter, J.W.F. Valle, Phys. Rev. D 25 (1982) 774.

[17] T. Hambye, E. Ma, U. Sarkar, Nucl. Phys. B 602 (2001) 23, arXiv:hep-ph/0011192.

[18] E. Ma, S. Sarkar, U. Sarkar, Phys. Lett. B 458 (1999) 73, arXiv:hep-ph/9812276;

P.H. Gu, M. Hirsch, U. Sarkar, J.W.F. Valle, Phys. Rev. D 79 (2009) 033010, arXiv:0811.0953 [hep-ph].
[19] T. Hambye, G. Senjanovic, Phys. Lett. B 582 (2004) 73–81, arXiv:hep-ph/0307237 [hep-ph].
[20] T. Hambye, New J. Phys. 14 (2012) 125014, arXiv:1212.2888 [hep-ph].
[21] T. Hambye, K. Kannike, E. Ma, M. Raidal, Phys. Rev. D 75 (2007) 095003, arXiv:hep-ph/0609228 [hep-ph].
[22] T. Hambye, M. Raidal, A. Strumia, Phys. Lett. B 632 (2006) 667–674, arXiv:hep-ph/0510008 [hep-ph].
[23] T. Hambye, Nucl. Phys. B, Proc. Suppl. 145 (2005) 280–285.
[24] P.H. Gu, E. Ma, U. Sarkar, Phys. Rev. D 94 (11) (2016) 111701, arXiv:1608.02118 [hep-ph].
[25] C. Alduino, et al., CUORE Collaboration, Phys. Rev. Lett. 120 (2018) 132501;
M. Agoshini, et al., GERDA Collaboration, Phys. Rev. Lett. 120 (2018) 132503;
C.E. Aalseth, et al., MAJORANA Collaboration, Phys. Rev. Lett. 120 (2018) 132502;
A. Gando, et al., KamLAND-Zen Collaboration, Phys. Rev. Lett. 117 (2016) 082503;
J.B. Albert, et al., EXO-200 Collaboration, Phys. Rev. Lett. 120 (2018) 072701;
G. Anton, et al., EXO-200 Collaboration, Phys. Rev. Lett. 123 (2019) 161802.
[26] K.R.S. Balaji, A. Dighe, R.N. Mohapatra, M.K. Parida, Phys. Rev. Lett. 84 (2000) 5034–5037, arXiv:hep-ph/0001310;
K.R.S. Balaji, A.S. Dighe, R.N. Mohapatra, M.K. Parida, Phys. Lett. B 481 (2000) 33–38, arXiv:hep-ph/0002177;
K.R.S. Balaji, R.N. Mohapatra, M.K. Parida, E.A. Paschos, Phys. Rev. D 63 (2001) 113002, arXiv:hep-ph/0011263.
[27] R.N. Mohapatra, M.K. Parida, G. Rajasekaran, Phys. Rev. D 69 (2004) 053007, arXiv:hep-ph/0301234;
R.N. Mohapatra, M.K. Parida, G. Rajasekaran, Phys. Rev. D 71 (2005) 057301, arXiv:hep-ph/0501275;
R.N. Mohapatra, M.K. Parida, G. Rajasekaran, Phys. Rev. D 72 (2005) 013002, arXiv:hep-ph/0504236;
S. Agarwalla, M.K. Parida, R.N. Mohapatra, G. Rajasekaran, Phys. Rev. D 75 (2007) 033007, arXiv:hep-ph/0611225;
W.G. Hollik, Phys. Rev. D 91 (3) (2015) 033001, arXiv:1412.4585 [hep-ph].
[28] S. Vaqnozzi, et al., Phys. Rev. D 94 (2016) 083522, arXiv:1605.04320 [astro-ph.CO];
S. Vaqnozzi, et al., Phys. Rev. D 96 (2017) 123503, arXiv:1701.08172 [astro-ph.CO];
S. Vaqnozzi, et al., Phys. Rev. D 98 (2018) 123526, arXiv:1802.08694 [astro-ph.CO].
[29] M. Ghosh, T. Ohlsson, S. Rosauro-Alcaraz, J. High Energy Phys. 03 (2020) 026, arXiv:1912.10010 [hep-ph];
S. Choubey, T. Ohlsson, Phys. Lett. B 739 (2014) 357–364, arXiv:1410.0410 [hep-ph].
[30] M. Aker, et al., KATRIN, Phys. Rev. Lett. 123 (22) (2019) 221802, arXiv:1909.06048 [hep-ex].
[31] D. Aristizabal Sierra, M. Dhen, T. Hambye, J. Cosmol. Astropart. Phys. 1408 (2014) 003, arXiv:1401.4347 [hep-ph].
[32] D. Aristizabal Sierra, F. Bazzocchi, I. de Mederios Verzilas, Nucl. Phys. B 858 (2012) 196, arXiv:1112.1843 [hep-ph];
D. Aristizabal Sierra, L.A. Munoz, E. Nardi, Phys. Rev. D 80 (2009) 016007;
D. Aristizabal Sierra, M. Losado, E. Nardi, J. Cosmol. Astropart. Phys. 0912 (2009) 015, arXiv:0905.0662.
[33] M. Chakraborty, M.K. Parida, B. Sahoo, J. Cosmol. Astropart. Phys. 01 (2020) 049, arXiv:1906.05601 [hep-ph].
[34] S. Davidson, A. Ibarra, Phys. Lett. B 535 (2002) 25–32, arXiv:hep-ph/0202239 [hep-ph].
[35] M.Yu. Khlopov, A.D. Linde, Phys. Lett. B 138 (1984) 265;
J. Ellis, J. Kim, D.V. Nanopoulos, Phys. Lett. B 145 (1984) 181;
J. Ellis, G.B. Gelmini, J.L. Lopez, D.V. Nanopoulos, S. Sarkar, Nucl. Phys. B 373 (1992) 399;
M. Kawasaki, T. Moroi, Prog. Theor. Phys. 93 (1995) 879;
V.S. Rychkov, A. Strumia, Phys. Rev. D 75 (2007) 075001.
[36] M. Drees, arXiv:hep-ph/9611409 [hep-ph].
[37] F. Vissani, Phys. Rev. D 57 (1998) 7027–7030, arXiv:hep-ph/9709409 [hep-ph].
[38] J.A. Casas, J.R. Espinosa, I. Hidalgo, J. High Energy Phys. 11 (2004) 057, arXiv:hep-ph/0410298 [hep-ph];
M. Farina, D. Pappadopulo, A. Strummia, J. High Energy Phys. 08 (2013) 022, arXiv:1303.7244 [hep-ph];
J.D. Clarke, R. Foot, R.R. Volkas, Phys. Rev. D 91 (2015) 073009, arXiv:1502.01352 [hep-ph];
M. Fabbrichesi, A. Urbano, Phys. Rev. D 92 (2015) 015028, arXiv:1504.05403 [hep-ph];
J.D. Clarke, R. Foot, R.R. Volkas, Phys. Rev. D 92 (2015) 033006, arXiv:1505.05744 [hep-ph].
[39] D.S. Akerib, et al., LUX Collaboration, Phys. Rev. Lett. 118 (2) (2017) 021303, arXiv:1608.07648 [astro-ph.CO].
[40] E. Aprile, et al., XENON Collaboration, Phys. Rev. Lett. 119 (18) (2017) 181301, arXiv:1705.06655 [astro-ph.CO].
[41] E. Aprile, et al., XENON Collaboration, Phys. Rev. Lett. 121 (11) (2018) 111302, arXiv:1805.12562 [astro-ph.CO].
[42] X. Cui, et al., PandaX-II Collaboration, Phys. Rev. Lett. 119 (18) (2017) 181302, arXiv:1708.06917 [astro-ph.CO].
[43] WMAP Collaboration, D.N. Spergel, et al., Astrophys. J. Suppl. 170 (2007) 377, arXiv:astro-ph/0603449 [INSPIRE];
D. Larson, J. Dunkley, G. Hinshaw, E. Komatsu, M.R. Nolta, C.L. Bennett, B. Gold, M. Halpern, et al., Astrophys. J. Suppl. 192 (2011) 16, arXiv:1001.4635 [astro-ph.CO].

[44] J. Elias-Miro, J.R. Espinosa, G.F. Giudice, H.M. Lee, A. Strumia, J. High Energy Phys. 06 (2012) 031, arXiv:1203.0237 [hep-ph].
[45] O. Lebedev, Eur. Phys. J. C 72 (2012) 2058, arXiv:1203.0156 [hep-ph].
[46] B.W. Lee, S. Weinberg, Phys. Rev. Lett. 39 (1977) 165–168;
K. Griest, M. Kamionkowski, Phys. Rev. Lett. 64 (1990) 615.
[47] P. Athron, et al., GAMBIT, Eur. Phys. J. C 77 (8) (2017) 568, arXiv:1705.07931 [hep-ph].
[48] J. Beringer, et al., Particle Data Group, Phys. Rev. D 86 (2012) 010001;
C. Patrignani, et al., Particle Data Group, Chin. Phys. C 40 (10) (2016) 100001.
[49] B. Sahoo, M. Chakraborty, M.K. Parida, Adv. High Energy Phys. 2018 (2018) 4078657, arXiv:1804.01803 [hep-ph].
[50] E. Ma, Phys. Rev. D 73 (2006) 077301, arXiv:hep-ph/0601225 [hep-ph].
[51] M.K. Parida, Phys. Lett. B 704 (2011) 206–210, arXiv:1106.4137 [hep-ph].
[52] T. Hambye, PoS IDM2010 (2011) 098, arXiv:1012.4587 [hep-ph];
M. Frigerio, T. Hambye, Phys. Rev. D 81 (2010) 075002, arXiv:0912.1545 [hep-ph].
[53] M. Kadastik, K. Kannike, M. Raidal, Phys. Rev. D 80 (2009) 085020, arXiv:0907.1894 [hep-ph];
M. Kadastik, K. Kannike, M. Raidal, Phys. Rev. D 81 (2010) 015002, arXiv:0903.2475 [hep-ph].
[54] E. Ma, Phys. Rev. D 98 (9) (2018) 091701, arXiv:1809.03974 [hep-ph].
[55] E. Ma, arXiv:2004.12949 [hep-ph].
[56] E.W. Kolb, M.S. Turner, Front. Phys. 69 (1990) 1.
[57] G. Bertone, D. Hooper, J. Silk, Phys. Rep. 405 (2005) 279, arXiv:hep-ph/0404175.
[58] P. Gondolo, G. Gelmini, Nucl. Phys. B 360 (1991) 145.
[59] J. McDonald, Phys. Rev. D 50 (1994) 3637, arXiv:hep-ph/0702143.
[60] W.L. Guo, Y.L. Wu, J. High Energy Phys. 1010 (2010) 083, arXiv:1006.2518 [hep-ph].
[61] A. Biswas, D. Majumdar, Pramana 80 (2013) 539, arXiv:1102.3024 [hep-ph].
[62] J.M. Cline, K. Kainulainen, P. Scott, C. Weniger, Phys. Rev. D 88 (2013) 055025, Erratum: Phys. Rev. D 92 (3) (2015) 039906, arXiv:1306.4710 [hep-ph].
[63] M. Chabab, M.C. Peyranere, L. Rahili, Phys. Rev. D 93 (11) (2016) 115021, arXiv:1512.07280 [hep-ph].
[64] N. Haba, H. Ishida, N. Okada, Y. Yamaguchi, Eur. Phys. J. C 76 (6) (2016) 333, arXiv:1601.05217 [hep-ph];
R. Padhan, D. Das, M. Mitra, A. Kumar Nayak, Phys. Rev. D 101 (7) (2020) 075050, arXiv:1909.10495 [hep-ph].
[65] I. Garg, S. Goswami, K.N. Vishnudath, N. Khan, Phys. Rev. D 96 (2017) 055020, arXiv:1706.08851 [hep-ph];
M. Gonderinger, Y. Li, H. Patel, M.J. Ramsey-Musolf, J. High Energy Phys. 1001 (2010) 053;
C.S. Chen, Y. Tang, J. High Energy Phys. 1204 (2012) 019, arXiv:1202.5717 [hep-ph];
N. Khan, S. Rakshit, Phys. Rev. D 90 (11) (2014) 113008, arXiv:1407.6015 [hep-ph].
[66] K. Kannike, Eur. Phys. J. C 76 (6) (2016) 324, arXiv:1603.02680 [hep-ph];
K. Kannike, Eur. Phys. J. C 72 (2012) 2093, arXiv:1205.3781 [hep-ph].
[67] G. Aad, et al., ATLAS CMS, Phys. Rev. Lett. 114 (2015) 191803, arXiv:1503.07589 [hep-ex].
[68] CDF, CMS ATLAS, D0, arXiv:1403.4427 [hep-ex].
[69] K.A. Olive, et al., Particle Data Group, Chin. Phys. C 38 (2014) 090001;
S. Bethke, Nucl. Phys. B, Proc. Suppl. 234 (2013) 229–234, arXiv:1210.0325 [hep-ex].
[70] P.A.R. Ade, et al., Planck, Astron. Astrophys. 571 (2014) A16, arXiv:1303.5076 [astro-ph.CO].
[71] Z.z. Xing, Prog. Theor. Phys. Suppl. 180 (2009) 112–127, arXiv:0905.3903 [hep-ph].
[72] P.S.B. Dev, C.M. Vila, W. Rodejohann, Nucl. Phys. B 921 (2017) 436–453, arXiv:1703.00828 [hep-ph].
[73] C. Bonilla, R.M. Fonseca, J.W.F. Valle, Phys. Rev. D 92 (2015) 075028, arXiv:1508.02323 [hep-ph];
A. Arhrib, R. Benbrik, M. Chabab, G. Moultaka, M.C. Peyranere, L. Rahili, J. Ramadan, Phys. Rev. D 84 (2011) 095005, arXiv:1105.1925 [hep-ph];
D. Das, A. Santamaria, Phys. Rev. D 94 (2016) 015015, arXiv:1604.08099 [hep-ph].
[74] Guillem Domieênech, Mark Godsell, Christof Wetterich, arXiv:2008.04310 [hep-ph].
[75] M. Cirelli, N. Forengo, A. Strummia, Nucl. Phys. B 753 (2006) 178.
[76] T. Hambye, M.H. Tytgat, Phys. Lett. B 659 (2008) 651–655, arXiv:0707.0633 [hep-ph];
R. Barbieri, L.J. Hall, V. Rychkov, Phys. Rev. D 74 (2006) 015007, arXiv:hep-ph/0603188.
[77] L.M. Krauss, F. Wilczek, Phys. Rev. Lett. 62 (1989) 1221.
[78] M.K. Parida, P.K. Sahu, K. Bora, Phys. Rev. D 83 (2011) 093004, arXiv:1011.4577 [hep-ph].
[79] M.K. Parida, R. Samantaray, Eur. Phys. J. Spec. Top. (2020), in press, accepted manuscript no. epjst2000024, arXiv:2002.06869 [hep-ph].